Communications Research Centre

VHF ADAPTIVE ANTENNA DEVELOPMENT TASK: FINAL REPORT (U)

by

R.W. Jenkins, U.A. Tenne-Sens and B. Lisson

COMMUNICATIONS RESEARCH CENTRE INDUSTRY AND SCIENCE
CRC REPORT NO. 93-003

June 1993
Ottawa

Government of Canada
Department of Communications

Gouvernement du Canada
Ministère des Communications

The work described in this document was sponsored by the Department of National Defence under Task 1410-0417W

Canada

VHF ADAPTIVE ANTENNA DEVELOPMENT TASK: FINAL REPORT (U)

by

R.W. Jenkins, U.A. Tenne-Sens and B. Lisson
Radio Communications Technology Directorate

The work described in this document was sponsored by the Department of National Defence under Task 1410-0417W

COMMUNICATIONS RESEARCH CENTRE INDUSTRY AND SCIENCE
CRC REPORT NO. 93-003

Canada

June 1993
Ottawa

ABSTRACT

The work of the VHF adaptive antenna development task is reported. An adaptive-antenna test bed was assembled, including a programmable real-time signal processing system. Power-ratio-inversion (PRI) and eigenvector-weighting (EV) adaptive algorithms were investigated analytically and by means of simulation, and implemented in two-element form on the real-time processor. These algorithms tend to separate incoming signals into different output channels according to their relative strengths, and do not require a priori information on the communications signal being received. The PRI algorithm was expected to invert the relative input powers of the jamming and communications signal, in the output signal. Analyses indicate that the EV algorithm should perform better than the PRI algorithm, especially when the incoming jamming and communications signals are well-separated in direction. Tests with real-world signals reveal deficiencies in the hardware implementation, as well as limitations in the algorithms themselves. Means of correcting the deficiencies are identified, and proposed for a new real-time signal processor to be implemented as part of a continuing technology-base activity. More effective algorithms which make use of a priori information on the communications signal to obtain a reference signal are recommended for implementation in the continuing work, the goal of which is to produce a demonstrable effective VHF adaptive-antenna system for land-tactical communications.

RÉSUMÉ

Ce rapport présente les résultats du projet de développement d'un système adaptif d'antennes pour les communications aux fréquences VHF. Un banc d'essai pour systèmes adaptifs d'antennes fut construit, incluant un système programmable de traitement des signaux en temps réel. Les algorithmes adaptifs d'inversion de puissance (PRI) at de balance des eigenvecteurs (EV) furent étudiés soit par analyse, soit par simulation, et furent implantés, pour deux antennes, dans le système programmable. Ces algorithmes ont tendance à séparer en deux canaux les signaux qui arrivent à la sortie du système, selon les puissances relatives, et ne nécessitent aucune connaissance "a priori" des caractéristiques de ces signaux. On s'attendait à ce que l'algorithme PRI inverse les puissances relatives des signaux de brouillage et de communications. L'analyse a indiqué que l'algorithme EV devrait fonctionner mieux que l'algorithme PRI, particulièrement lorsque les signaux de brouillage et de communications sont bien séparés en direction. Des essais avec des signaux réels ont révélés des lacunes dans le matériel et des limitations dans les algorithmes. Nous identifions ici des moyens pour corriger ces lacunes et proposons de réaliser un nouveau processeur de traitement des signaux sous un projet de technologie de base. Ce nouvel effort comprendra la réalisation d'algorithmes qui utilisent des caractéristiques connues "a priori" du signal désiré pour ainsi obtenir un signal de référence. Le but final est de démontrer la faisabilité d'un système efficace adaptif d'antennes VHF pour les communications terrestres militaires.

EXECUTIVE SUMMARY

This report summarizes the work performed at CRC under the VHF adaptive antenna development task. This work is directed toward providing an antijamming capability for VHF land-tactical communications. As presently envisaged, this capability would be provided by a specially built receiving system consisting of two (or more, if desired) antennas, commonly tuned receiver front ends, and a digitally implemented programmable signal processor. This system would be capable of receiving and deciphering communications signals from the new combat net radio under development, as well as performing interference cancellation according to a variety of stored algorithms, each appropriate to a particular communications signal format or operational situation that might be encountered.

A major part of the task was the development of a VHF adaptive antenna test bed. In addition to the appropriate transmitting and receiving equipment, a programmable real-time signal-processing system was assembled. This system was used to implement candidate adaptive antenna algorithms. It permitted these algorithms to be tested with real signals, as well as with simulated signals generated by specially written software. The signal-simulation software provided a way to extend the testing to conditions that otherwise may not have been possible with the real-signal tests, and also permitted precise and repeatable test conditions, against which different techniques could be compared. A description of the test bed and its associated software is contained in this report.

Due to PY limitations the work of the present task was restricted to investigating a particular class of algorithms which tend to separate incoming signals into separate output channels. These algorithms are quite flexible in the types of communication signals they can work with, and are appropriate for the FM voice signals currently employed for VHF land-tactical communications. A two-element array was used for the actual implementation of the algorithms; the analysis and modelling also considered more elements.

The first algorithm to be considered was the power-ratio-inversion (PRI) algorithm, which has the property of inverting the relative powers of jamming and communications signals seen at the input. This algorithm has been implemented in analog form in earlier adaptive antenna systems; it is limited in its interference cancellation when the jamming and communications signals are close in power. The second algorithm considered was the eigenvector-weighting (EV) algorithm, which has up to now received little attention. Analyses of the EV algorithm reveal that in many cases, the EV algorithm performs better than the PRI algorithm, often yielding adequate performance with the jamming and communications close in power. However, the EV algorithm performance improves as the number of antenna elements increases, and for a two-element array there remains a substantial fraction of possible cases for which the achieved interference cancellation is inadequate.

The implemented PRI and EV algorithms were tested against simulated signals and found to perform according to the expectations of theory. Tests with real-world signals revealed adaptive-antenna effects, due to the hardware implementation, which limited performance. These included receiver mismatches introduced mainly in the final-stage filters of the receive channels, receiver phase noise, and analog-to-digital quantization noise. These effects acted to limit the

operating range, over which the adaptive antenna system could be effective, to jamming signal levels no more than 20 to 25 dB stronger than the wanted signal.

It is planned to carry on the VHF adaptive antenna work started in the present task under the current adaptive antenna technology-base activity, with the goal of producing a demonstrable effective system for land-tactical use.

Plans include the replacement of the programmable signal processing system with a new low-cost PC-based system that has become technically feasible since the original system was developed. This system will permit the final receiver filtering to be performed digitally, thus remedying the receiver mismatch problem. It will have more bits available for analog to digital conversion, thereby reducing quantization noise. Receiver phase noise will be eliminated as a problem by running the receivers from a common local oscillator. This system should become the basis of a demonstrable adaptive antenna system, for land-tactical use.

The new system will be based on Texas Instruments TMS320C40 digital signal-processing chip technology, which can be incorporated into operational systems thus permitting the operational software developed under the present program to be transferred with minimal cost. Similar technology is being incorporated into an HF adaptive antenna system developed for naval communications. This will facilitate the sharing of software between the VHF and HF applications.

More effective algorithms which require predetermined knowledge of portions of the communications signal will be implemented in the new system. These algorithms are signal-specific, and are well-suited to the newer forms of data signalling now coming into use. An existing highly effective algorithm developed at CRC for the NATO STANAG 4285 HF serial waveform will be adapted to similarly-structured VHF signals.

TABLE OF CONTENTS

1.0 INTRODUCTION

The VHF Adaptive Antenna Development Task was originally intended to develop an interference-cancelling adaptive antenna system for application to the new VHF combat net radio (CNR). Previous modelling and analytic studies had shown it to be an effective antijamming technique for the land-tactical environment. The first and funded portion of this task, as described in phases 1 and 2 of the task description sheet, include the development of an adaptive-antenna test bed and the identification, test-bed implementation and testing of appropriate adaptive techniques in order to establish their feasibility. It is this work that the present report covers.

The latter part of the task was dependent on decisions taken regarding the CNR architecture. The decision was made to procure an existing design for the CNR that was not amenable to incorporating adaptive-antenna technology. As a result, the emphasis of the task shifted from a system that was embedded as part of the new CNR to a stand-alone system that would receive signals from a CNR but not depend on a CNR for its implementation. Such a system might be installed in vehicles or at fixed ground sites where more than one antenna could be justified. As a result of this decision, it became appropriate to terminate the development task at the end of its current funding and continue work under an existing adaptive-antenna technology-base program, to the point where an implementable system could be demonstrated and a decision regarding final operational development and purchase could be made.

This report is intended as both a final report on the VHF development task, and a progress report on the work being done at CRC to address the DND requirement for interference cancellation on VHF land-tactical communications circuits.

Section 2 describes the adaptive-antenna test bed. This includes a description of the hardware, including a programmable real-time processing system, which was the major component developed in the test-bed system. System software, including signal simulation and algorithm evaluation software, are described.

The algorithms implemented and tested were those which tended to separate the incoming signals at the output, and which did not require a priori information on the communications signal. This strategy is appropriate for the FM voice signals employed in land-tactical VHF communications. A two-element adaptive array is the most likely configuration, given the limited space available on vehicles. A power-ratio inversion (PRI) algorithm and eigenvector-weighting (EV) algorithm were implemented for this array. Sections 3 and 4 describe the PRI algorithm and EV algorithms respectively, and review their performances against simulated signals.

Section 5 reviews the test-bed measurements with real-world signals, using both the PRI and EV algorithms. These measurements provided not only a test of the algorithms, but of the hardware implementation. Various deficiencies in the hardware and algorithms as implemented are identified.

The conclusions of the work are provided in Section 6. These include recommendations for overcoming the identified deficiencies, and the work planned for the next phase, to be carried out under the technology base program.

2.0 VHF ADAPTIVE-ANTENNA TEST BED

A major initiative in the VHF Adaptive Antenna Development Task has been the implementation of an adaptive-antenna test bed. The test bed was developed to further test and develop adaptive-antenna algorithms and techniques prior to their implementation in operational prototypes, and to gain experience in issues of implementation.

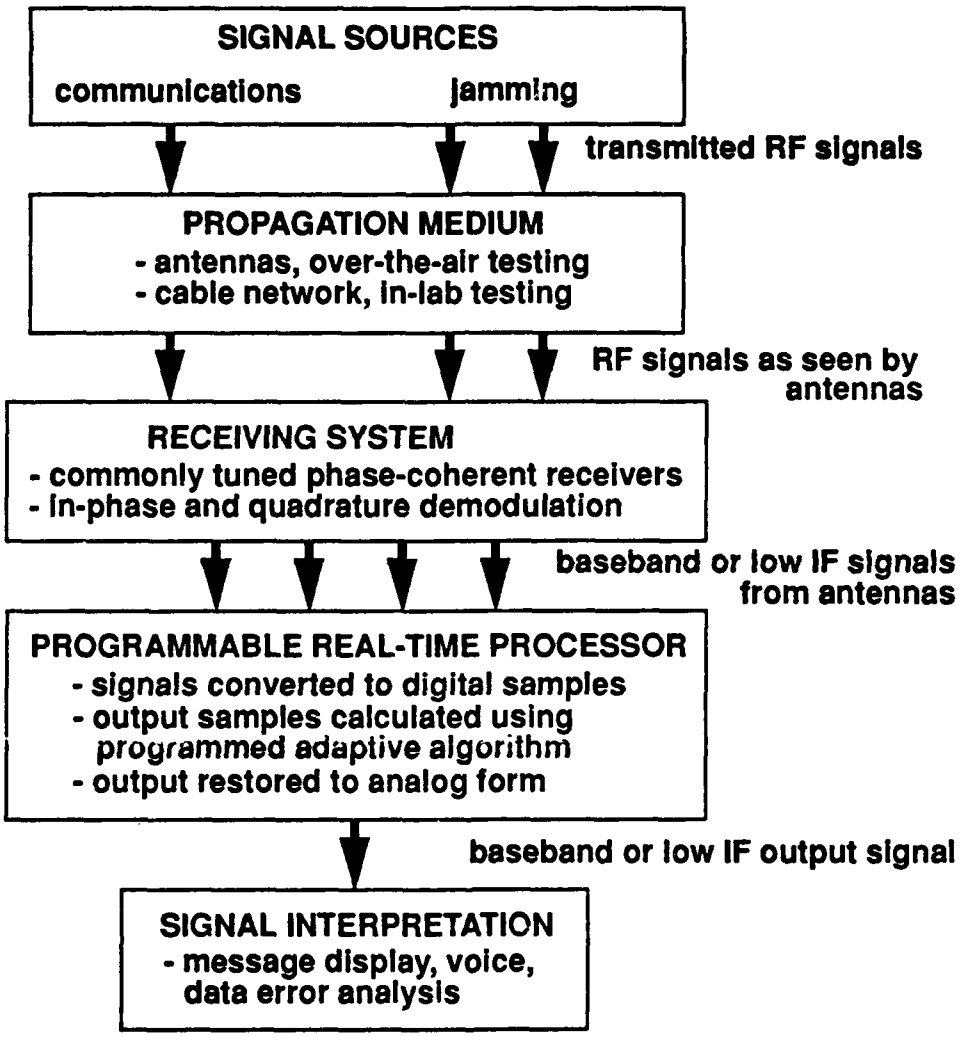

Figure 2.1 VHF adaptive-antenna test bed.

The test bed is illustrated in Figure 2.1. It consists of jamming and communications signal sources, a receiving system including four commonly tuned receivers, and a programmable real-time processor. It is intended to be highly flexible so as to accommodate a wide variety of fixed-frequency and frequency-hopping applications, and adaptation techniques.

RF signals from the communications and jamming sources are passed to the receivers,

either over the air with the aid of transmitting and receiving antennas, or in the lab via a specially built network of variable-length cables and power splitters/combiners which simulate an antenna array receiving the signals from different directions. The operating frequency range includes but is not restricted to the 30-88 MHz VHF land-mobile band.

The programmable real-time processor is a major portion of the test bed. This system accepts either baseband or low-IF signals from the receivers, and converts them to digital samples for processing. Eight input channels are available, permitting in-phase and quadrature signals from up to four antennas, or IF signals from up to eight antennas, to be sampled. After digital conversion, the processor calculates weights from the input signals and then applies these weights to the input signals and combines the weighted signals to form output signal samples, which are then converted back into an analog signal. The weights calculation and weighting operations are carried out according to programs which are written on and stored in the processing system. The processing system is high-speed, so that it will operate in real time and perform as an adaptive-array processor in field tests, thus enabling the evaluation of adaptive-antenna algorithms.

As well as working with real signals, the processing system may be used in non-real time with stored signal samples, previously generated internally by signal simulation software. The software-generated samples provide a means of quickly testing programmed adaptive-antenna techniques without setting up other test-bed equipment. This capability permits different techniques to be tested against the same precisely specified conditions, and it extends operating conditions beyond those readily available in field tests.

2.1 VHF RECEIVING SYSTEM

The VHF receiving system, shown in Figure 2.2, receives the signals transmitted in free space in over-the-air experiments, or via cables in in-lab experiments, and demodulates them to baseband or low-IF frequencies.

The receivers used for this purpose are four Watkins-Johnson WJ-8628A-1 intercept and monitor receivers in a WJ-9040 equipment frame. The frame includes the common power supply, a site-lockable frequency reference module, and IEEE 488 bus control. These receivers were selected on the basis of their low phase noise, ability to accept external local oscillator signals (permitting noise-free phase-coherent operation), and ability to operate with frequency-hopping signals. The receivers can be run coherently using internally-set tuning (and local oscillator signals) and a common external frequency reference. This is the mode of operation illustrated in Figure 2.2. The 10-MHz frequency reference output of an HP 8645A frequency synthesizer provides the reference frequency. A PC computer is used to control the receivers' RF frequency, gain, and IF bandwidth, via the IEEE-488 bus.

The receivers' 21.4-MHz IF output is passed to a specially built I-Q demodulation system, which reduces the signals to baseband in-phase (I) and quadrature (Q) signals. This demodulation system uses a HP 3335A frequency synthesizer to produce a 21.4-MHz CW tone which is used in the frequency down-conversion process. The 21.4-MHz tone is also locked to the 10-MHz frequency reference.

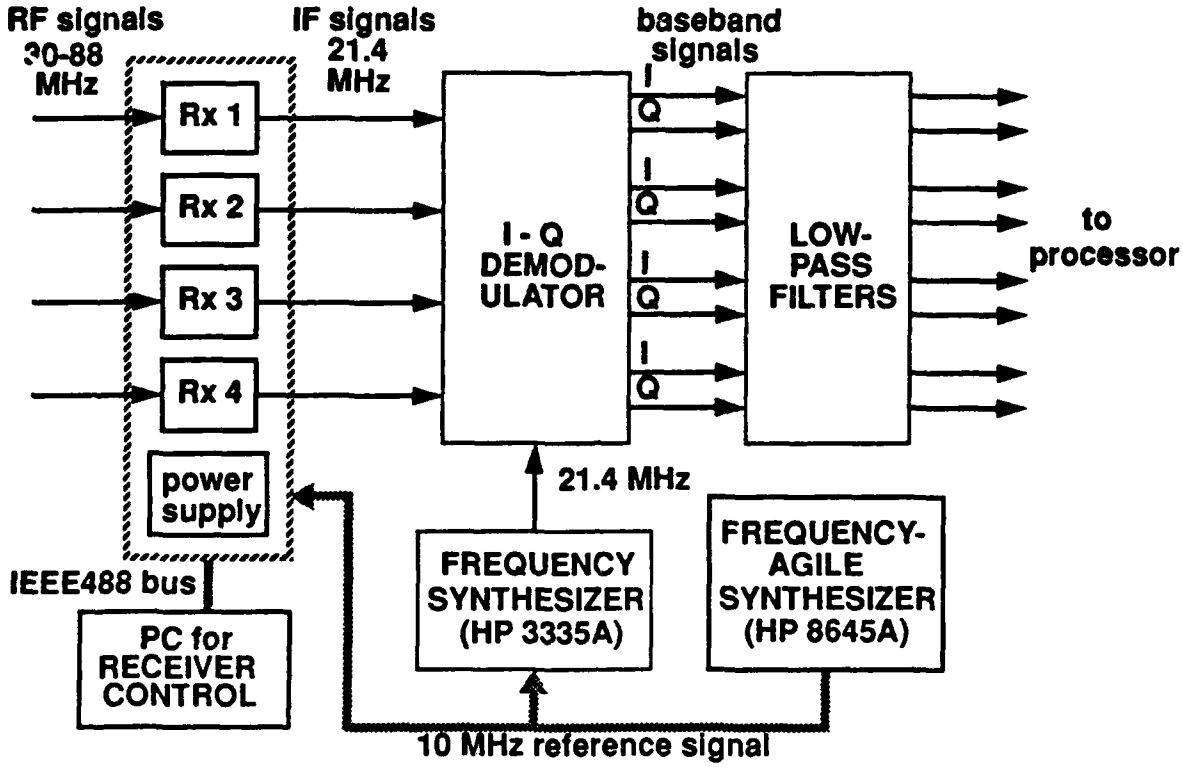

Figure 2.2 Receiving system.

The resultant baseband in-phase and quadrature signals are passed through a set of precision low-pass filters, before being sent to the programmable processor. The input bandwidth of the signal to the processor is set by these filters, which have cutoff frequencies selectable over the 10-Hz to 150-kHz range. Typical settings were 6.0 and 12.5 kHz, corresponding to bandwidths of 12 and 25 kHz, respectively.

Frequency hopping is facilitated by an external local oscillator signal from a HP 8645A frequency-agile frequency synthesizer. This synthesizer has a tuning time of less than 0.1 ms, and so can support hop rates up to 10 kilohops/sec. A second HP 8645A synthesizer provides a frequency-hopping capability at the transmitter.

The I-Q demodulator is shown in more detail in Figure 2.3. The 21.4 MHz reference tone is amplified by 15 dB, then split into two components I_{osc} and Q_{osc} with one shifted 90° with respect to the other. Each of these components is then split into four, to provide I_{osc} and Q_{osc} signals for up to four receivers.

The upper part of Figure 2.3 shows the first receiver path in more detail; the other three paths are identical. The 21.4-MHz IF signal from the receiver is amplified by 16 dB, then split into two. One branch is mixed down to baseband with the I_{osc} signal, the other with the Q_{osc}

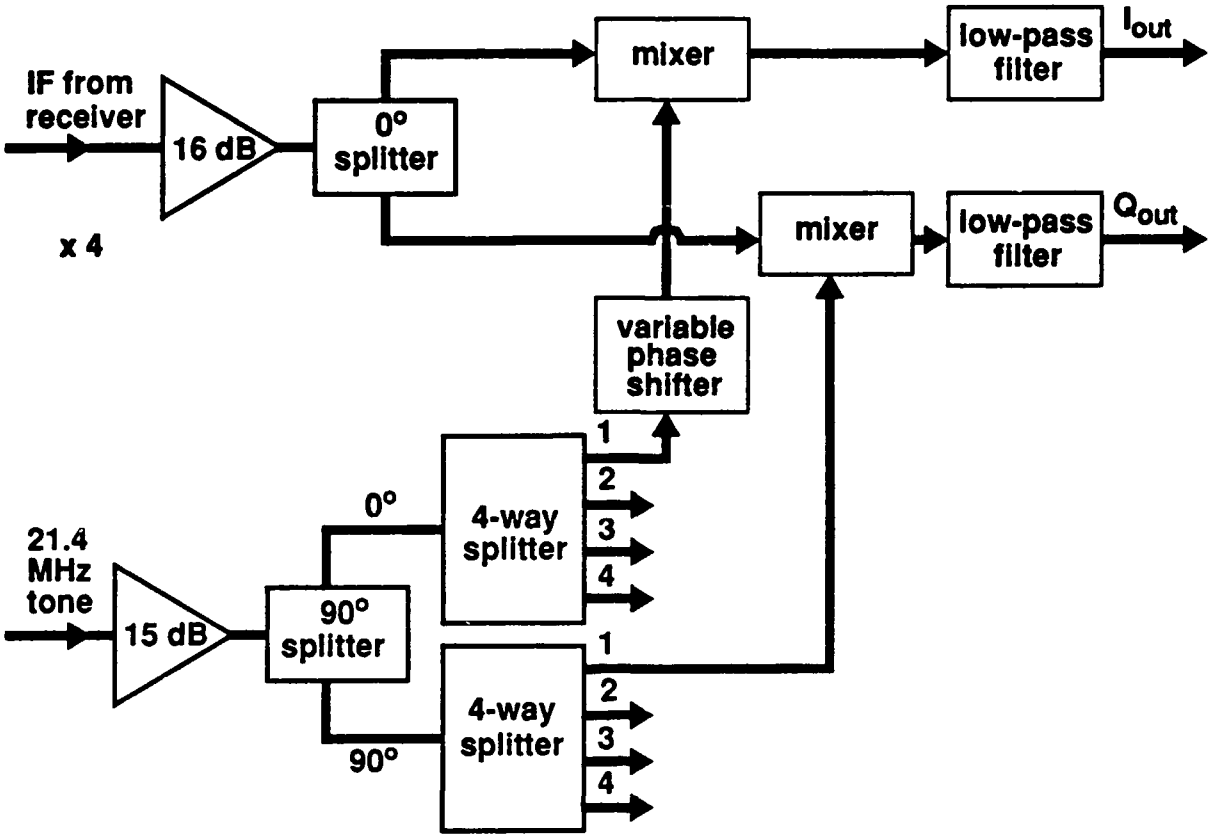

Figure 2.3 I-Q demodulator

signal. These signals are then passed to low-pass filters to remove the higher-frequency component (42.8 MHz) of the mixing, resulting in the baseband in-phase (I) and quadrature (Q) signals.

A variable phase shifter in the I_{osc} branch permits fine adjustment of the relative phases of the I and Q signals, in order to compensate for asymmetries in the 0° splitter and mixers, and inaccuracy in the 90° splitter.

2.2 PROGRAMMABLE REAL-TIME PROCESSOR

The programmable processor provides a means of implementing adaptive-antenna algorithms for test purposes. A functional block diagram of this processor is provided in Figure 2.4. Input baseband or low IF signals from the receivers are sampled and converted to numbers, which are accumulated into blocks of operator-specified length. When a block has been accumulated, it is ready for processing. When the input process is ready, the block is transferred into memory and processed according to the adaptive algorithm being tested. The result is a set of weights for the block, used to weight and sum the input samples in the block, thus producing a

block of output samples. The block of output samples is passed to the output process where it is restored to serial format and converted back to an analog signal.

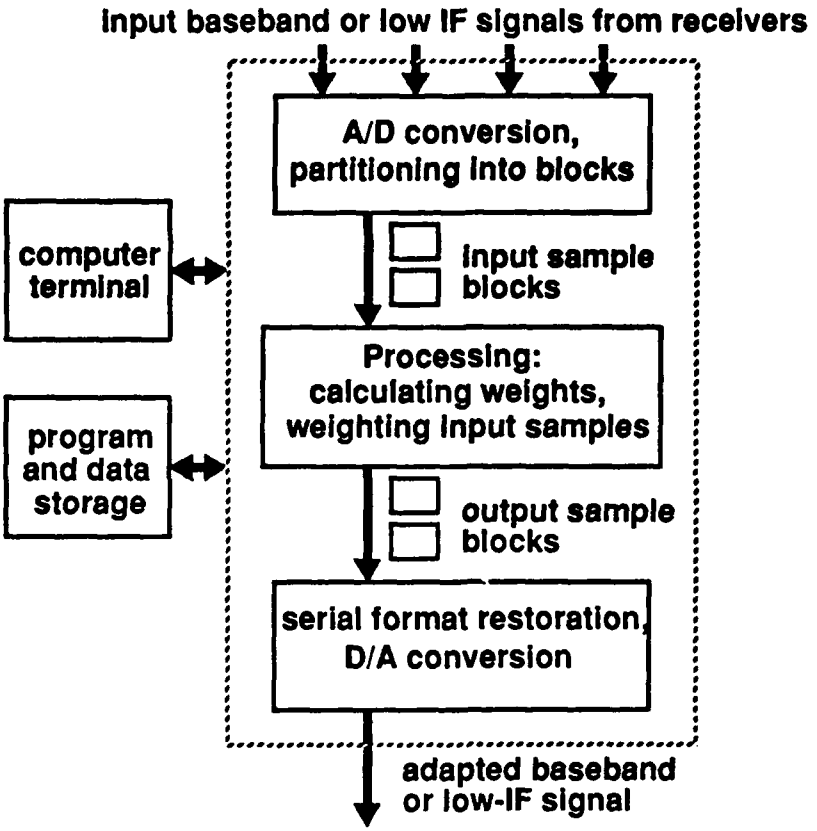

Figure 2.4 Programmable real-time adaptive-antenna processor: functional block diagram.

The programmable nature of the processor is facilitated by the inclusion of a terminal which provides an operator interface, and various magnetic media which provide program and data storage, backup, and program input. As part of its function, the processor is required to operate as a general-purpose computer for the development of operating programs, signal simulation programs, and performance evaluation routines.

2.2.1 Hardware

A block diagram of the processor system hardware is shown in Figure 2.5. Essentially the system consists of three parts: host, input/output, and processing. Where possible, off-the-shelf components were used to implement these subsystems.

The host, or controller subsystem, includes a MicroVAX II computer in a specially built enclosure with enough power, cooling, and empty slots to accommodate the other portions of the system. Communications between the cards in the enclosure are provided by Q-bus. A computer terminal provides the necessary operator interface; a hard disk, the program and data storage; a streaming tape unit provides system backup, and a floppy disk drive provides backup and entry of

smaller program and data files. Additional ports permit a printer to be attached, as well as additional terminals, so that more than one user can access the host for program development.

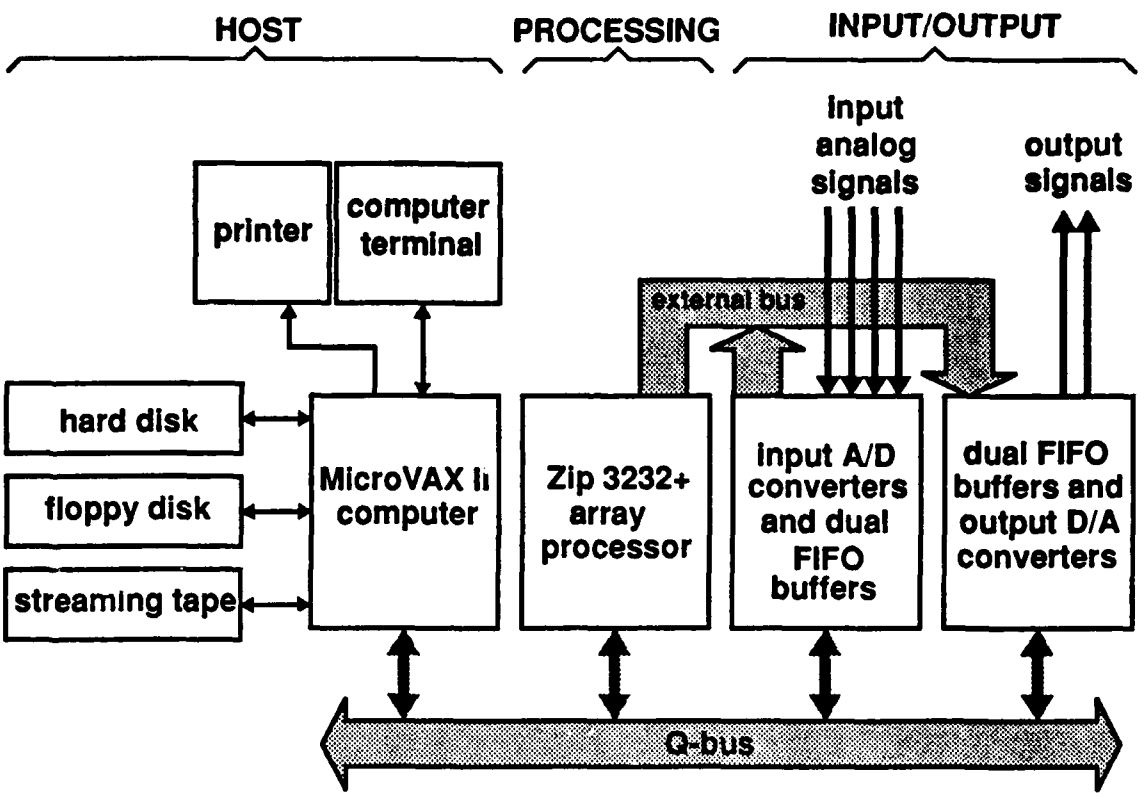

Figure 2.5 Programmable real-time processor: hardware block diagram.

The input/output (I/O) subsystem handles the input of signals from the receivers and the output of corresponding processed signals. It consists of two sets of cards, for input and output. These cards were designed and built at CRC, as there were no suitable commercial products at the time.

The input portion can accommodate up to eight input channels. On each channel, a sample- and-hold circuit samples the signal according to a programmed delay, following a common sample-timing signal. Twelve-bit analog-to-digital (A/D) converters convert the signal samples from the channels into numbers, which are then stored sequentially in FIFO (first-in, first-out) memory. When a programmed number of samples has been stored, the FIFO memory is swapped with a second FIFO memory, and the samples for that block passed to the processing subsystem, via an external port. The second FIFO memory meanwhile accepts new samples so that there is no loss in continuity. In addition to these functions, communications is provided with the host via the Q-bus, for the setting of operating parameters such as the number of input channels, the block length, and the sampling delay for each channel. The input portion is controlled by a TMS320C20 processor, run according to a program stored in read-only memory (ROM).

The output cards provide a similar set of functions, in reverse order. A block of processed samples is passed when it is ready, by the host to the available FIFO memory in the output portion. Meanwhile a second FIFO memory is having its stored samples read out sequentially, according to the original sample timing, to a set of 16-bit D/A converters. Up to four analog output channels are available. Following conversion, the output signals are then low-pass filtered to remove quantization noise.

The I/O subsystem has two modes of operation: continuous and pulsed. The continuous mode is the conventional mode of operation; in this mode, input signals are sampled and passed to the processing subsystem in blocks continuously. The pulsed mode is intended for frequency-hopping applications. In the pulsed mode, sampling is initiated by the reception of an external pulse (coincident with a frequency change), starting a specified time after the pulse and lasting for a specified number of blocks.

The processing subsystem consists of a Mercury Zip 3232+ processor, which appears to the host MicroVAX as an input/output (I/O) device. The Zip processor is designed for high-speed floating operations, and has a maximum speed of 20 Mflops. It includes a control processor which handles most of the I/O and logic operations of the programs, and two dual-pipeline arithmetic processors which operate in parallel, performing the same programmed operations on different data. It also includes a 2-Mbyte program and data memory, as well as smaller immediately accessible program memories and data registers in the control and arithmetic processors. A major function of the control processor is to move data between the 2-Mbyte memory and the arithmetic processor registers. Once initiated and provided with data, the arithmetic processors perform their operations in parallel with those of the control processor.

In a typical operation, the operating program is loaded into the Zip by the host and the Zip started, to run unattended. The loaded program coordinates its operation with those of the host and I/O subsystems by the use of interrupts.

2.2.2 Software

The software resident on the programmable processor can be divided into two groups according to use: development and operation.

The development software is the commercial software normally available on a general-purpose computer for program development, and is run on the MicroVax host. It includes the C and Fortran languages, and the MicroVMS operating system. It also includes the development software for the Mercury Zip array processor: a compiler and assembler, a standard algorithm library of commonly used mathematical routines, and a simulation package facilitating the debugging of programs written for the Zip. In addition, there is a set of custom-written drivers for the I/O boards, which are used in test programs for these boards, as well as in the normal operation of these boards. These drivers permit a user to control the I/O operating parameters of these boards, to enter simulated data into their dual FIFOs, to examine and clear the contents of the FIFOs, to start and stop the sampling of signals, and to reset the operating programs resident in their ROM memories.

The operational software is those programs and data files specific to the actual operation of the processor as an adaptive antenna system. It includes the adaptive-antenna program resident in the Zip processor, the host-resident control program, and parameter files which provide initial settings for the operating array which are read and passed by the host program to the Zip program and I/O boards. In addition it includes a signal simulation program and parameter files, and performance evaluation programs. The I/O board drivers mentioned previously are also used by the host-resident control program to control these boards. The remainder of this section discusses the operational software.

The host program permits the operator to run the programmable processing system as an adaptive array processor and to control and monitor its operation. It was written to be quite general, so that different adaptive-antenna algorithms (prepared as Zip programs) can be run from the same host program with very little modification. A self-explanatory block diagram of the host program's operation is provided in Figure 2.6. It is intended to start up the adaptive antenna processing, and provide communications between the operator and the rest of the system during operation. Initial operational parameters are entered from a previously written file; individual parameter values may be changed by the operator prior to and during operation.

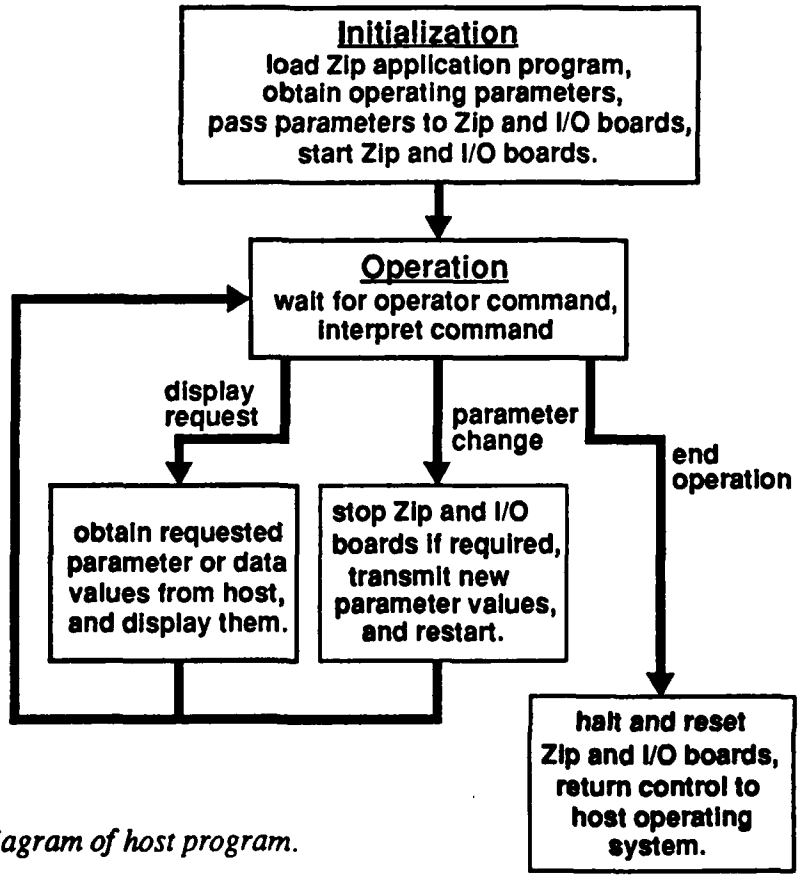

Figure 2.6 Block diagram of host program.

The Zip-resident program includes the adaptation algorithm and other associated signal processing performed by the system. Its details depend on the technique being implemented. At present, PRI and EV algorithms have been implemented as programs, for two-antenna systems. Despite the algorithm dependency, these Zip programs have a common structure and use similar routines for communicating with the rest of the adaptive-antenna processing system. This structure is illustrated in Figure 2.7.

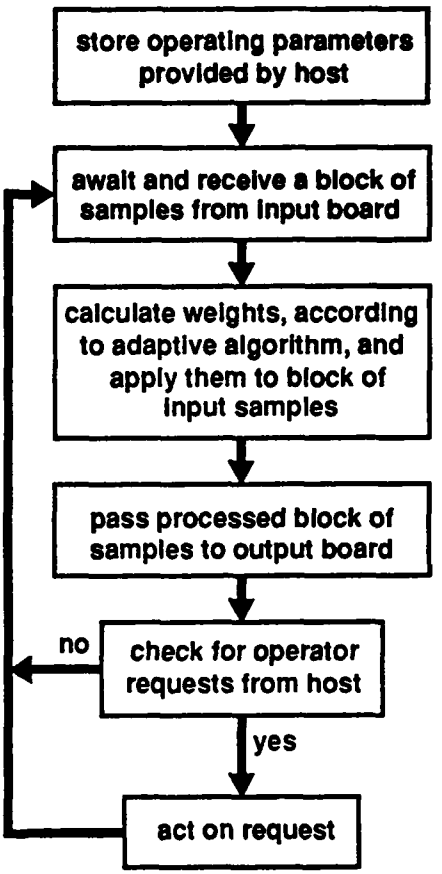

Figure 2.7 Structure of Zip adaptive-antenna real-time processing program.

As illustrated in this figure, the initial action of the Zip program upon being started is to initialize itself, and store the operating parameters that were passed to it by the host program, prior to its start-up. The program then awaits a signal from the input board that a block of samples is ready, and reads them into memory. It uses these samples to calculate weights, and then weights and combines the same samples to obtain a block of output samples. It then alerts the output board, and upon receipt of a ready signal from the output board, passes the processed output samples. At this point it has done everything it can with the received samples. It uses the remaining time to check if an operator request has been made via the host program. This could be a simple parameter or data display request, a parameter change request, or a shutdown request. In the case of a data or parameter display request, the information is sent to the host. In the case of a parameter change, the program operation is suspended to allow transfer of the changed parameter from the host to the Zip, following which operation is resumed. At that point, or if no request has been made, the program returns to wait for a new block of samples.

In order to exercise the adaptive-antenna processing system without providing real signals, and also to provide perfectly controllable and repeatable scenarios, a signal simulation software package was developed. The operation and major elements of this package are illustrated in Figure 2.8.

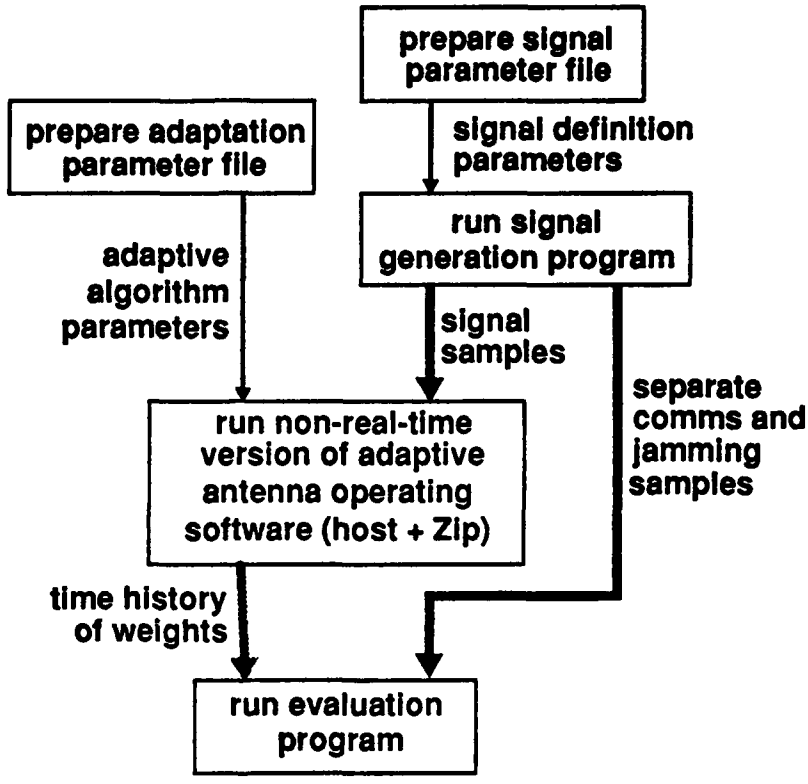

Figure 2.8 Operation of adaptive antenna processor with simulated signal data

The simulation package includes a signal generation program that simulates incoming communications, jamming, and noise signals, and calculates files of 12-bit data samples similar to those that would emerge from the D/A converters in a real-signal test. These signals are prepared according to signal definition parameters contained in a parameter file which can be altered by the operator at will. The samples are assumed to be baseband in-phase and quadrature. In addition, a file of the separate communications, jamming, and noise components of the samples (as floating-point numbers) is prepared. This last file is used in evaluating algorithm performance.

After a set of simulated signals has been prepared, it can be used as input to a non-real-time version of the adaptive-antenna host and Zip programs. These programs are obtained from the real-time versions with a small amount of modification. The non-real-time host program obtains the operating parameters, and sets up the non-real-time Zip program to run with these parameters. It then starts the Zip program, which awaits a transfer of input signal samples from the host. The host program reads the first block of input samples from the sample file, and transmits them to the Zip program for processing, to produce a set of weights. These are passed to the host to be written to an output file. (The output samples are derived, but not used in this case.)

The host program then reads another block of input samples and passes them to the Zip which processes them, returning another set of weights. This procedure is repeated until the file of simulated signal samples has been completely read. The result of this process is a time history of the weights, one set per block, obtained from the input samples.

The final stage of the simulation process is that of evaluation. The evaluation program opens the file of weights generated by the non-real-time adaptive-antenna programs and reads the first set of weights. It also opens the file of separate communications, jamming, and noise component signals generated by the signal generation program, and reads in the first block of these components. The weights are applied to these components to obtain the average input and output communications, jamming, and noise powers S(in), J(in), N(in), S(out), J(out), N(out) for the first block. The input and output signal-to-noise-plus-jamming ratios SNIR(in) and SNIR(out) are computed, as is the processing gain G = SNIR(out)/SNIR(in). The program then reads the weights derived for the next block of samples, and the next block of separate communications, jamming, and noise component samples. The procedure is repeated until all the blocks of weights and samples have been read. The program then computes the means and rms deviations, of S(in), J(in), N(in), S(out), J(out), N(out), SNIR(in), SNIR(out) and G over the entire run. These quantities, along with the block-by-block values, are written to an output file and displayed on the terminal.

The signal simulation software permits a variable antenna-array geometry, operating frequency, signal directions, and communications and jamming signal characteristics. Up to five separate jamming signals may be defined, and their signals strengths specified. The communications signal type is assumed to be BPSK, of variable baud rate, while the jamming signals may be pure-tone or white-noise, continuous or pulsed. The sample rate and total number of samples to be generated is also under operator control. In addition, each of the signals may be specified to have a multipath component of arbitrary amplitude, direction, and Doppler shift.

3.0 PRI ALGORITHM

3.1 OVERVIEW

The PRI algorithm, implemented here in two-element form, is really a special case of the constrained SMI (sample-matrix inversion) algorithm described by Horowitz et al.[1]. It requires no a priori knowledge of the received signals and, in the presence of two signals of dissimilar input power, has the effect of inverting their relative powers at the output [2]. Thus it can be expected to be effective in situations where there exists a single interfering signal that is substantially stronger than the desired signal; in other situations it will be ineffective.

The two-element PRI algorithm involves only simple calculations and can easily be implemented with analogue components as well as in digital form. It has been used in commercially available 2-element systems [3]. For our purposes, it provided a basis of comparison with other techniques, and also provided a first test of the programmable development system itself.

3.2 POTENTIAL FOR LAND-TACTICAL RADIO

In the land tactical radio environment, the platforms concerned are likely to be moving vehicles, and multipath propagation is present. These two characteristics ensure that the signals will be fading relative to each other. In addition, the signal strength is a strong function of the distance from the transmitter. Therefore, the jamming may be significantly stronger than communications only for some stations in a net, and even for these stations, there will be times, due to fading, where the jamming drops below the communications signal level. Because of its power-inverting properties, the PRI algorithm is expected to experience dropouts under such conditions.

3.3 THEORY

The output signal y is described in terms of the input signals x_1 and x_2 from the two antennas, and the corresponding weights w_1 and w_2, as follows:

$$y = \hat{w}_1 x_1 + \hat{w}_2 x_2 \tag{3.1}$$

where x_1 and x_2 are baseband complex signals, and the weights are likewise complex with ^ representing the complex conjugate. If the first weight is constrained to unity, the output is given by

$$y = x_1 + \hat{w}_2 x_2 \tag{3.2}$$

and the output power P, by

$$P = \overline{\hat{y}y} = \overline{\hat{x}_1 x_1} + \hat{w}_2 \overline{\hat{x}_1 x_2} + w_2 \overline{\hat{x}_2 x_1} + \hat{w}_2 w_2 \overline{\hat{x}_2 x_2} \tag{3.3}$$

where $\overline{xx}$ refers to a statistical average. P is a quadratic function of the weight w_2 and therefore has a single minimum, where $\frac{\partial P}{\partial \hat{w}_2} = 0$.

The free weight w_2 is adjusted to minimize the output power. By differentiating equation (3.3) and equating the result to zero, the following is obtained:

$$\frac{\partial P}{\partial \hat{w}_2} = 0 = \overline{\hat{x}_1 x_2} + w_2 \overline{\hat{x}_2 x_2} \tag{3.4}$$

Rearranging equation (3.4), the solution for the weight is found:

$$w_2 = -(\overline{\hat{x}_1 x_2}) / (\overline{\hat{x}_2 x_2}) \tag{3.5}$$

The present implementation uses equations (3.2) and (3.5) to obtain the output signal. The statistical average represented by $\overline{xx}$ in (3.5) is replaced by summation over a number (block) of input samples, plus block to block averaging of the form

$$(new) = \alpha\,(old) + (1-\alpha)\,(block) \tag{3.6}$$

where (old) refers to the average for the previous block, $(block)$ refers to the block-derived estimate, and (new) refers to the average for the present block. The parameter α is related to a time constant T_0 (measured in blocks) by

$$\alpha = \frac{T_0}{1+T_0} \tag{3.7}$$

Equation (3.7) is used in the implementation to obtain α from the operator-entered block averaging time constant T_0.

3.4 SIMULATION PROCEDURE

The simulation procedure consisted of the following steps:

(a) generating files of signal samples. This was done by running the program SIGNAL4, which produced a predetermined number of samples, according to the array and signal parameters provided. As well as producing a set of resultant 12-bit samples representing the composite signals at the array, this program also produced sets of floating-point samples corresponding to each of communications, jamming, and noise signals separately. These floating-point numbers were required for evaluation purposes.

(b) running the PRI program against the signal samples. The simulation version of the PRI program, stored under PRIHOSTSIM (for the host MicroVAX computer) and PRIWTSIM (for the actual Zip application program) was run for specified operator-defined parameters, block size and averaging time constant. This produced a file which contained, among other things, the set of weights obtained for each block of input samples.

(c) evaluating the result. This was done by running the program PRIEVAL, which processed the input floating-point samples according to the weights obtained for each block, for each of the communications, jamming and noise signals, and then computed the output communications, jamming, and noise powers, the input and output signal-to-noise-plus-interference ratios SNIR(in) and SNIR(out), and the output phase (relative to input) of the communications. In addition to the block-by-block estimates, the mean values and rms variations of each of these quantities were computed.

3.4.1 Parameters

The simulations were carried out for the conditions described in Table 3.1.

Table 3.1 Parameters used in PRI algorithm simulations

operating frequency	60 MHz
2-element array spacing	3.0 m
receive filter bandwidth (3dB)	20 kHz
sampling rate	38.4k samples/s
communications signal	binary-phase-coded ASCII message ("The quick brown fox . . .")
communications bit rate	9600 bits/s
communications direction	normal to the array (0° incidence)
jamming signal	additive white gaussian noise, constant or pulsed
block length	64 samples

3.5 SIMULATION TEST RESULTS

Using the above signal and array parameters, the following sets of tests were performed:

3.5.1 Dependence of SNIR(out) on SIR(in)

The input signal-to-interference ratio SIR(in) was varied in 5-dB steps over the range -30 to +20 dB. The input noise power was assumed to be 20dB below that of the communications. The interference consisted of a constant-noise jamming signal, incident on the array at 45°. The PRI algorithm used an averaging time constant of $T_0 = 2$ blocks for this test. Each simulation was run for 2048 samples, or 32 blocks.

The resulting output signal-to-interference-plus-noise ratio SNIR(out) is plotted against SIR(in) in Figure 3.1. Both the mean values and rms variations of the block-by-block estimates are shown. Also shown in Figure 3.1 is the expected inverse relationship between SNIR(out) and SIR(in) in the absence of noise. A second line shows the limit set on SNIR(out) by the

background noise which is uncorrelated between antennas.

The mean simulation results are seen to follow the expected mean performance quite closely, for those values of SNIR(out) which are not limited by noise. The background noise becomes important where SNIR(out) is expected to approach or exceed 20 dB. For this region, the simulation values fall away from the expected noise-free values, remaining near 20 dB.

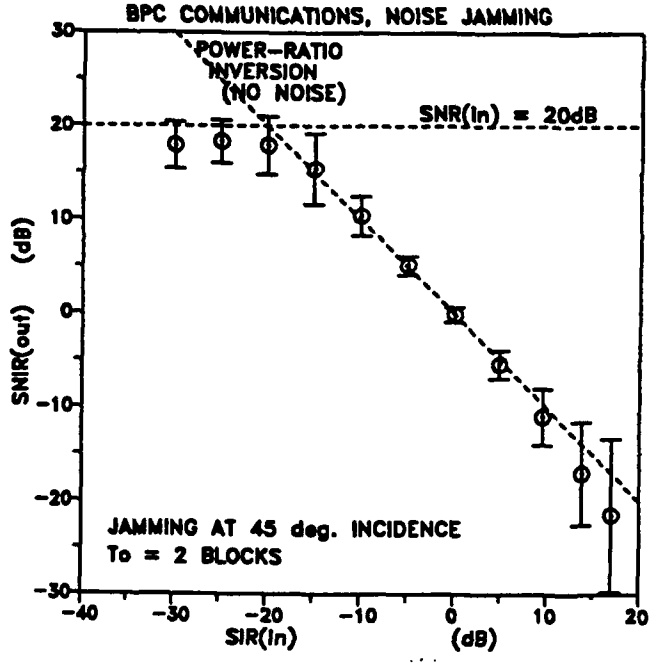

Figure 3.1. SNIR(out) as a function of SIR(in) for the PRI algorithm

The rms variation in block-by-block estimates increases when SIR(in) and SNIR(out) move away from 0 dB. The variations demonstrate that the performance for single blocks can exceed or be less than power inversion. On the average, the performance is equal to power inversion.

3.5.2 Dependence of SNIR(out) on Relative Signal Directions

To examine the PRI algorithm's dependence on angular separation, the jamming arrival direction was varied from 1° to 90° incidence, while the communications direction was kept at 0°. Simulations were run with the input jamming power 10 dB above the communications power, and background noise levels 15 and 30 dB below the communications. As for the previous test, the jamming was a constant-noise signal. An averaging time constant of 2 blocks was used for the PRI algorithm, and each simulation was run for 2048 samples.

The resulting performance in terms of SNIR(out) is plotted against the jamming incidence angle, in Figure 3.2. Results are shown for input signal-to-noise ratios SNR(in) of both 15 and 30 dB.

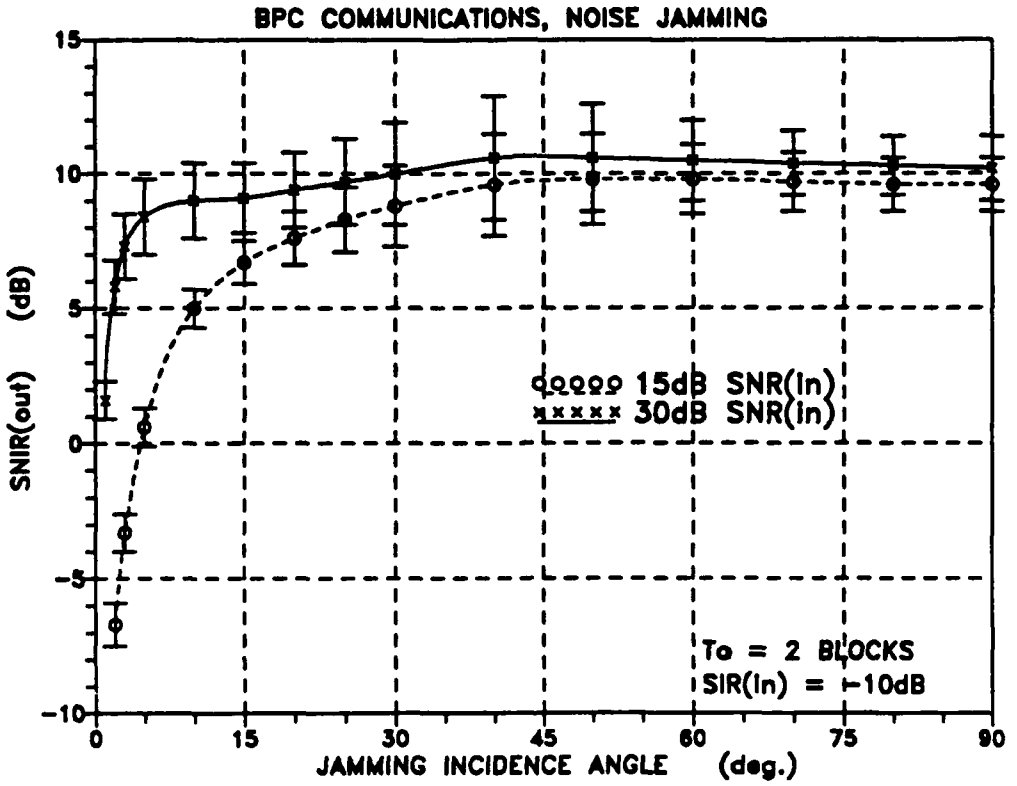

Figure 3.2 SNIR(out) as a function of jamming incidence angle for the PRI algorithm

For larger angular separations, the performance is that of power ratio inversion. However, when the jamming direction approaches that of the desired communications, the performance drops off. This is due to a reduction of gain in the communications direction as the jamming direction approaches it. The array gain for noise remains the same, and so SNR(out) and thus SNIR(out) is reduced. As expected, the performance drop-off is worse for the lower (15-dB) input signal-to-noise ratio.

3.5.3 Performance Against Time-Varying Jamming

In order to study the effect of time-varying signals on PRI adaptive-antenna performance, a pulsed-noise jamming signal of 50% duty cycle and 16-block period was introduced. The jamming angle of incidence was 45°. The simulation duration was lengthened to 4096 samples in order to cover several periods of pulsed jamming. A time-average signal-to-interference ratio

SIR(in) of 10 dB was used, and the input signal-to-noise ratio was 20 dB. Five averaging time constants were tried for the PRI algorithm: T_0 = 1, 2, 4, 8 and 16 blocks.

The resulting performance in terms of SNIR(out) is plotted as a function of time for the five averaging time constants, in Figure 3.3a. The corresponding communications-signal phase (relative to input) is plotted in Figure 3.3b. Figure 3.3b provides a measure of the phase modulation introduced on the communications signal by time variations in the weights (as they respond to the jamming). The on-off times for the pulsed jamming are indicated in these figures.

Two considerations help in understanding the resultant performance.

First, when only a communications signal and background noise are present, the PRI algorithm tends to cancel the communications signal, placing it below the noise level. Thus, when the jamming signal is pulsed, the communications signal will be cancelled during the jamming off-times, in the absence of any time averaging. When time-averaging is introduced, the weights formed during jamming off-times are partially based on past signals which include jamming-on times. Provided the averaging time constant is sufficiently large relative to the jamming off-time, the communications signal will not be cancelled during off-times, but will remain well above noise.

Second, when the averaging time constant is less than the jamming off-time, the weights at the end of the off-time will be derived from jamming signals whose power is much less than the average. When the jamming reappears, owing to the time averaging, the next set of weights will also be based on a small fraction of the average jamming power, despite the current incident jamming power exceeding the average. As a result, the performance obtained at these times will be less than that expected on the basis of the average signal powers alone.

These two effects are evident in Figures 3.3a and b. For the shortest averaging time constants (T_0 = 1, 2 blocks), the weights derived towards the end of the jamming off-times tend to cancel the communications signal, so that SNIR(out) drops well below 0 dB, and the output communications phase wanders. For a longer time constant that is still less than the jamming-off time (T_0 = 4 blocks), the performance at the reappearance of the jamming (following a jamming-off interval) reflects weights derived from signals acquired mainly in the absence of jamming, and the performance is well below the power inversion result. However, the output communications signal phase remains constant, unaffected by the time-varying jamming. As the averaging time constant T_0 is increased to values approaching and exceeding the jamming-off time (8, 16 blocks), the performance at the reappearance of jamming improves. This improvement is due to the weights being derived from a signal history that extends more into previous jamming-on times. For the longer averaging times, the performance during jamming-off times is that expected (~22 dB) on the basis of the input signal to noise ratio (20 dB) and the signal processing gain for the two-element array with a null in the jamming direction (~2 dB).

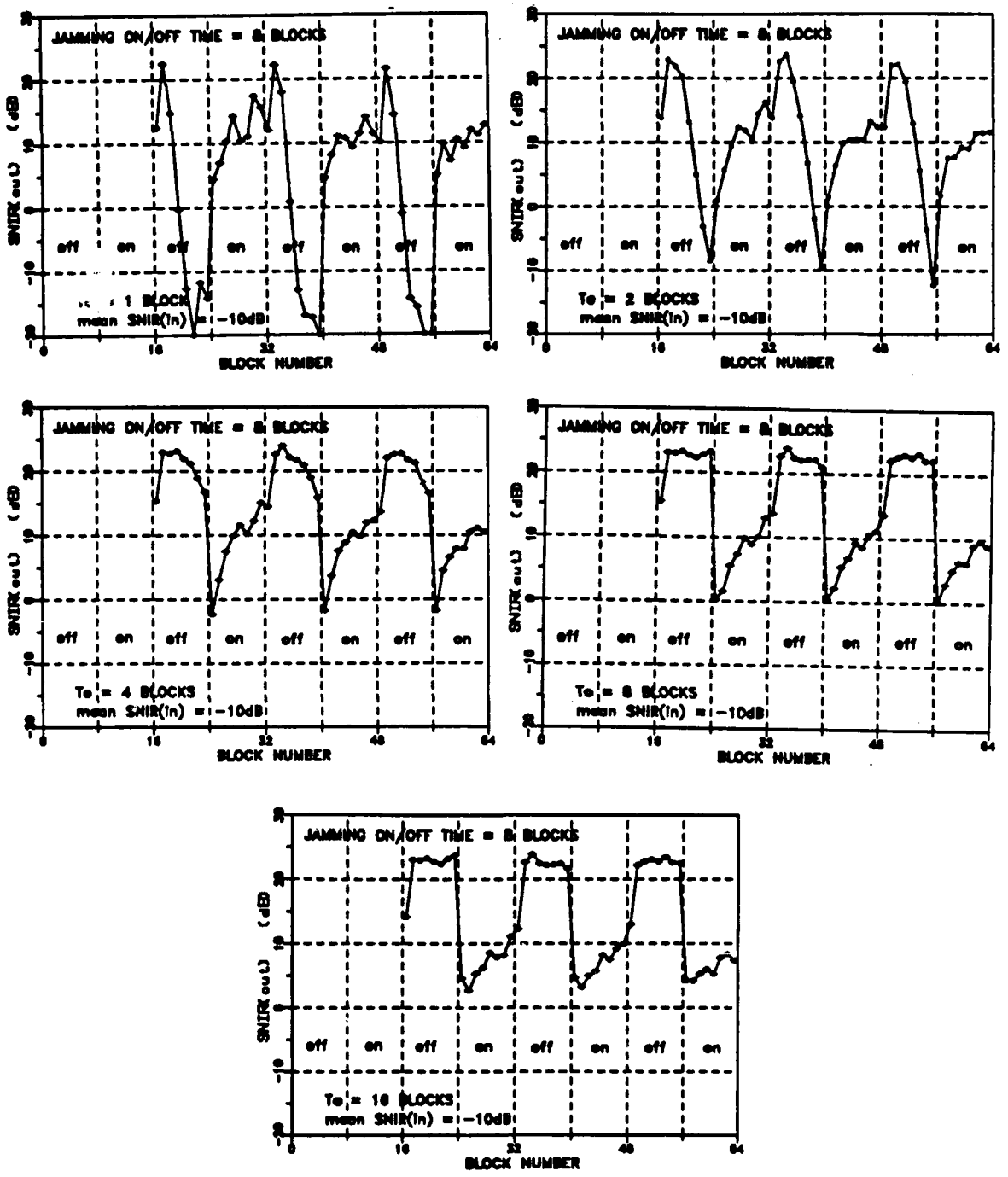

Figure 3.3a. Performance of the 2-element PRI adaptive-array algorithm, against pulsed-noise jamming, in terms of SNIR(out) as a function of time, for various averaging time constants.

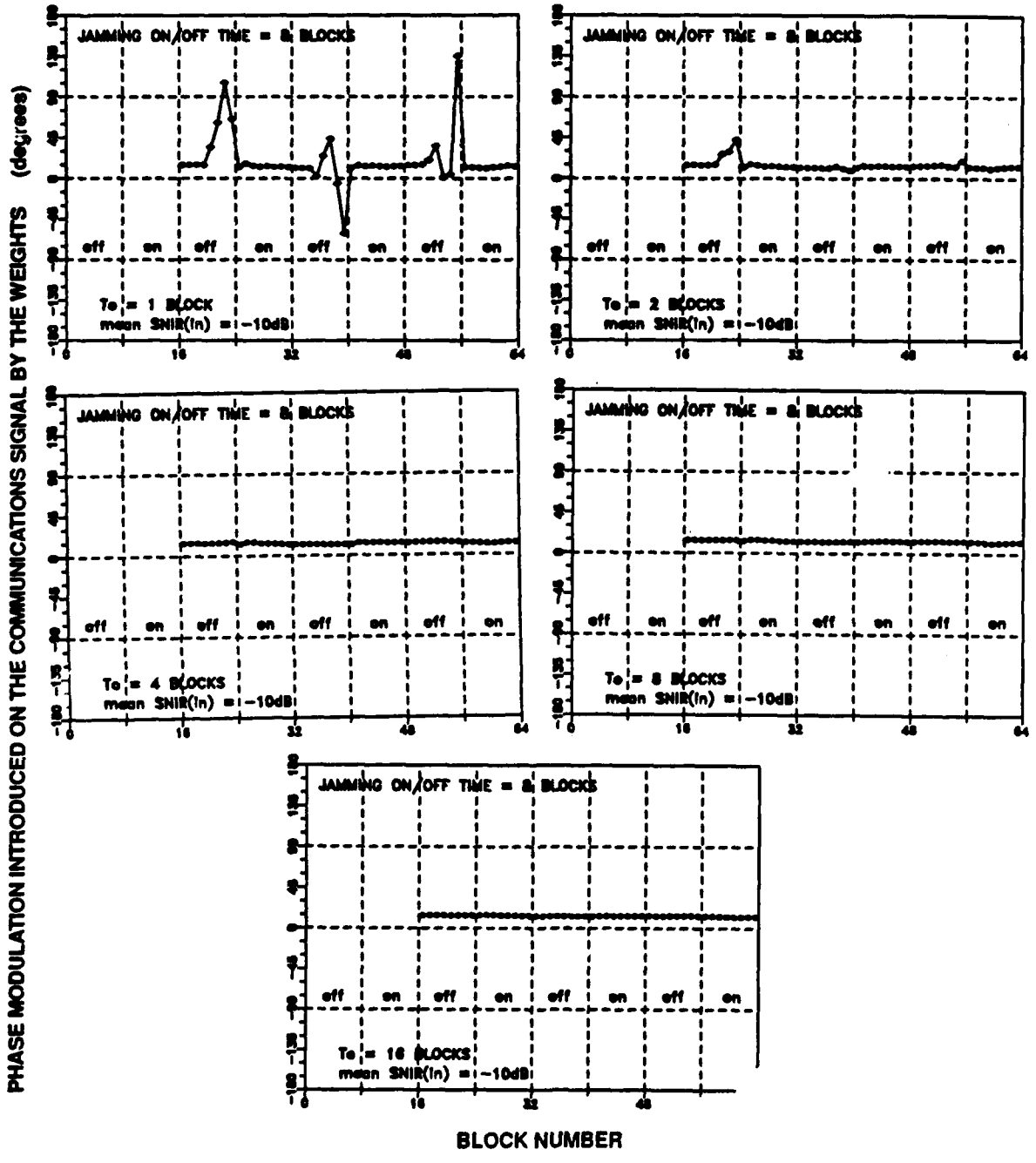

Figure 3.3b. Performance of the 2-element PRI adaptive array algorithm, against pulsed-noise jamming, in terms of the phase modulation introduced on the communications signal by the weights, as a function of time, for various averaging time constants.

3.6 SIMULATION FINDINGS

The PRI algorithm, implemented on the Zip array processor, performs according to the expectations of theory, and is not unduly limited by the implementation.

In a stationary-signal environment, its performance is limited by the power-inversion property, and by the input signal-to-noise ratio.

In a time-varying signal environment where fading or modulated jamming occurs, the power-inversion property of the PRI algorithm can at times give rise to poor performance. Provided the mean input interference power is substantially greater than that of the communications, the use of time-averaging may improve performance in these cases. The averaging times must approach or exceed the fading or jamming-off times for this to happen. At the same time, care must be taken that the averaging does not extend beyond the time over which the signal directions, or array orientation, can be considered to be constant.

4.0 EIGENVECTOR-WEIGHTING (EV) ALGORITHM

4.1 OVERVIEW

The eigenvector-weighting technique [2, 4] is a signal-separation technique, i.e., it tends to separate the signals arriving on the array into different output channels. The technique involves using each of the eigenvectors of the covariance matrix of the input signals from the antennas, as a set of weights which are applied to the input signals to form an output signal for that eigenvector.

The corresponding eigenvalues represent the powers of the respective output signals. If the eigenvectors, and thus output signals (or channels), are ordered according to the size of the eigenvalue from large to small, then the strongest incident signal will appear in the first output channel, the next strongest in the second channel, and so on until all signals have been accounted for. The remaining output channels contain noise only.

It has been shown in theory [2] that in the presence of a wanted signal and a single interfering signal, eigenvector weighting does at least as well as power inversion and, under certain conditions, much better. It has also been shown [2] that better performance is achieved when the signals from the input antennas have been received with equal gain.

In the present case a two-element algorithm is implemented. Thus a maximum of two signals may be separated. In cases where the interference is stronger than the communications, the communications will be in the second output channel. Otherwise, the communications will be in the first channel. Thus a decision is required as to which output channel to select. (This is similar to the PRI algorithm situation, where the choice is whether to use the algorithm output or that of the first input channel.)

4.2 POTENTIAL FOR LAND-TACTICAL RADIO

The strong dependence of signal strength on distance ensures that any jamming signal could, for the differently located receiving stations in a net, be either weaker or stronger than the desired communications. The fading conditions experienced with moving platforms makes it likely that the relative jamming and communications signal strengths will vary with time. Thus, any implementation of either the eigenvector-weighting (EV) algorithm or the PRI algorithm should have a way of selecting the appropriate output channel. Like the PRI algorithm, the EV algorithm will perform best when the interference and communications are well separated in power. When the two signals are close in power, the EV algorithm will sometimes work, unlike the PRI algorithm which always fails under these conditions.

4.3 THEORY

In this section, a brief overview of the general eigenvector weighting theory is given, followed by a description of the 2-element EV algorithm implementation.

A baseband complex representation is used for the signals. The input signals $\hat{x} = \begin{bmatrix} x_1 \\ x_2 \end{bmatrix}$ for the two input channels (i.e. element antennas) are combined to form a covariance matrix

$$\boldsymbol{R} = \overline{\hat{x}\hat{x}^H} = \begin{bmatrix} \overline{x_1\hat{x}_1} & \overline{x_1\hat{x}_2} \\ \overline{x_2\hat{x}_1} & \overline{x_2\hat{x}_2} \end{bmatrix} \tag{4.1}$$

where $\hat{x}$ represents a column vector, $\hat{x}$ a complex conjugate, and $\hat{x}^H$ the conjugate transpose. $\overline{xx}$ represents a statistical average, which is replaced in practice by a time average. Matrices are indicated by boldface capitals.

The eigenvectors $\hat{e}_i$ of the covariance matrix $\boldsymbol{R}$ are defined by the eigenvector equation

$$\boldsymbol{R}\hat{e}_i = \lambda_i\hat{e}_i\,, \quad i = 1, 2 \tag{4.2}$$

where λ_i are the corresponding eigenvalues. For a covariance matrix, λ_i can be shown to be real nonnegative. The eigenvectors can be made to be orthogonal, and can be normalized, to form an orthonormal set. The matrix $\boldsymbol{E}$ is defined as containing the eigenvectors as columns, i.e.,

$$\boldsymbol{E} = \begin{bmatrix} \hat{e}_1 & \hat{e}_2 \end{bmatrix} \tag{4.3}$$

and the eigenvector equation becomes

$$\boldsymbol{R}\boldsymbol{E} = \boldsymbol{E}\Lambda\,, \tag{4.4}$$

where Λ is the diagonal matrix of the eigenvalues: $\Lambda = \begin{bmatrix} \lambda_1 & 0 \\ 0 & \lambda_2 \end{bmatrix}$.

In the eigenvector-weighting technique, an eigenvector is used as a set of weights to weight and combine the input signals to produce a corresponding output

$$y_i = \hat{e}_i^{H}\hat{x}\,, \quad i = 1, 2\,. \tag{4.5}$$

The two outputs resulting from using the two eigenvectors as weights can be represented by a vector $\hat{y}$ given by

$$\hat{y} = \boldsymbol{E}^H\hat{x}\,. \tag{4.6}$$

The covariance matrix of the output signals is, from (4.4),

$$\boldsymbol{U} = \overline{\hat{y}\hat{y}^H} = \boldsymbol{E}^H\overline{\hat{x}\hat{x}^H}\boldsymbol{E} = \boldsymbol{E}^H\boldsymbol{R}\boldsymbol{E} = \boldsymbol{E}^H\boldsymbol{E}\Lambda = \Lambda\,, \tag{4.7}$$

since the columns of $\boldsymbol{E}$ form an orthonormal set of vectors. This says that the diagonal elements of $\boldsymbol{U}$, which are the powers in the two output channels, are the eigenvalues λ_1 and λ_2. Also, since Λ is a diagonal matrix, $\overline{y_1\hat{y}_2} = 0$, and the signals in the two output channels are uncorrelated.

In the EV implementation, the covariance matrix $\boldsymbol{R}$ is calculated by summing the correlation products over a block of samples. In a manner similar to the PRI implementation (Section 3.3), this block total is not used directly, but instead is averaged with the previous estimate for the last block of samples, to arrive at a new estimate for the current block, according to

$$\boldsymbol{R}\,(new) = \alpha \boldsymbol{R}\,(previous) + (1-\alpha)\,\boldsymbol{R}\,(block)\ , \tag{3.6}$$

where the parameter α lies between 0 and 1 and is related to a time constant T_0 (measured in blocks), by

$$\alpha = \frac{T_0}{1+T_0}\ . \tag{3.7}$$

In the implementation, T_0 and the number of samples in the block are operator-entered parameters.

Before the input signals are weighted and combined, the gains of the input channels are adjusted so that the input powers in the input channels are equal. This is an attempt, in the absence of other information, to make the input channel gains the same. Since the diagonal elements R_{11} and R_{22} of $\boldsymbol{R}$ are the input powers, this is easily done by setting the gains equal to

$$g_1 = \frac{1}{\sqrt{R_{11}}} \quad \text{and} \quad g_2 = \frac{1}{\sqrt{R_{22}}}\ , \tag{4.8}$$

so that the diagonal elements of the gain-compensated covariance matrix $\boldsymbol{R}'$ become unity. The eigenvector technique is then applied to the gain-adjusted inputs.

The eigenvalues can be found as the solutions to the equation

$$det\,[\boldsymbol{R}' - \lambda \boldsymbol{I}] = 0 \tag{4.9}$$

where *det* refers to the determinant, and $\boldsymbol{I}$ is the unit matrix. For the two-element case, where the gains have been adjusted according to equation (4.8) so that the diagonal elements of $\boldsymbol{R}'$ are unity, the solutions are

$$\lambda'_{1,2} = 1 \pm \frac{|R_{12}|}{\sqrt{R_{11}R_{22}}} \tag{4.10}$$

where R_{12} refers to the (1,2)th element of the uncompensated covariance matrix $\boldsymbol{R}$. The corresponding eigenvectors can be found from the eigenvector equation to within an arbitrary complex multiplicative factor. This factor is chosen for each eigenvector so that the first element is positive real and the magnitude of the eigenvector is one. The corresponding eigenvectors then become

$$\hat{e}'^{\,II}_{1,2} = \frac{1}{\sqrt{2}}\left[1, \pm\sqrt{\frac{\hat{R}_{12}}{R_{12}}}\right]\ . \tag{4.11}$$

In the present EV implementation, the output signals are normalized to ensure that the average power always lies within the range of the output digital-to-analog converter, by dividing the weights by the square roots of the eigenvalues (4.10). The corresponding weights, resulting from the input channel gain adjustment plus the eigenvector weighting followed by normalization, are given by

$$\vec{w}_{1,2}^{H} = \frac{1}{\sqrt{\lambda'_{1,2}}}\left[\frac{1}{\sqrt{2R_{11}}}, \pm\frac{R_{12}}{|R_{12}|\sqrt{2R_{22}}}\right] . \tag{4.12}$$

The output signals are found from the resultant weights and the original input signals, according to

$$y_{1,2} = \vec{w}_{1,2}^{H}\vec{x} . \tag{4.13}$$

4.4 SIMULATION PROCEDURE

The simulation procedure consisted of the following steps:

(a) generating files of signal samples. Signal sample files were generated using SIGNAL4, which produced a predetermined number of samples according to the array and signal parameters provided. As well as producing a set of resultant 12-bit samples representing the composite signals at the array, this program also produced sets of floating-point samples corresponding to each of communications, jamming, and noise signals separately. The floating point samples were required for evaluation purposes.

(b) running the EV program against the signal samples. The simulation version of the EV program, stored under EVHOSTSIM (for the host MicroVAX computer) and EVWTSIM (for the actual Zip application program), was run for specified operator-defined parameters: block size and averaging time constant. This produced a file which contained, among other things, the set of weights obtained for each block of input samples.

(c) evaluating the result. This was done by running the program EVEVAL, which processed the input floating-point samples according to the weights obtained for each block, for each of the communications, jamming and noise signals, to obtain the output communications, jamming, and noise powers, the output signal-to-noise-plus-interference ratio SNIR(out), and the output phase (relative to input) of the communications, for each of the two output channels. The input signal-to-noise-plus-interference ratio SNIR(in) was also computed for each block. In addition to the block-by-block estimates, the mean values and rms variations of each of these quantities were computed.

4.4.1 Parameters

The simulations were carried out for conditions similar to those of the PRI algorithm, described in Table 3.1. For convenience, the table is reproduced here.

Table 4.1 Parameters used in EV and PRI algorithm simulations

operating frequency	60 MHz
2-element array spacing	3.0 m
receive filter bandwidth (3dB)	20 kHz
sampling rate	38.4k samples/s
communications signal	binary-phase-coded ASCII message ("The quick brown fox . . .")
communications bit rate	9600 bits/s
communications direction	normal to the array (0° incidence)
jamming signal	additive white gaussian noise, constant or pulsed
block length	64 samples

4.5 SIMULATION TEST RESULTS

4.5.1 Dependence of SNIR(out) on Relative Signal Directions

The behaviour of the EV algorithm was examined as a function of input jamming direction, for input signal-to-interference ratios SIR(in) of -10 dB and -3 dB. Various averaging time constants T_0 of 1,2,4, and 8 blocks, were used for these tests. An input signal-to-noise ratio SNR(in) of 30 dB was used. The simulations were each run for 2048 samples, or 32 blocks.

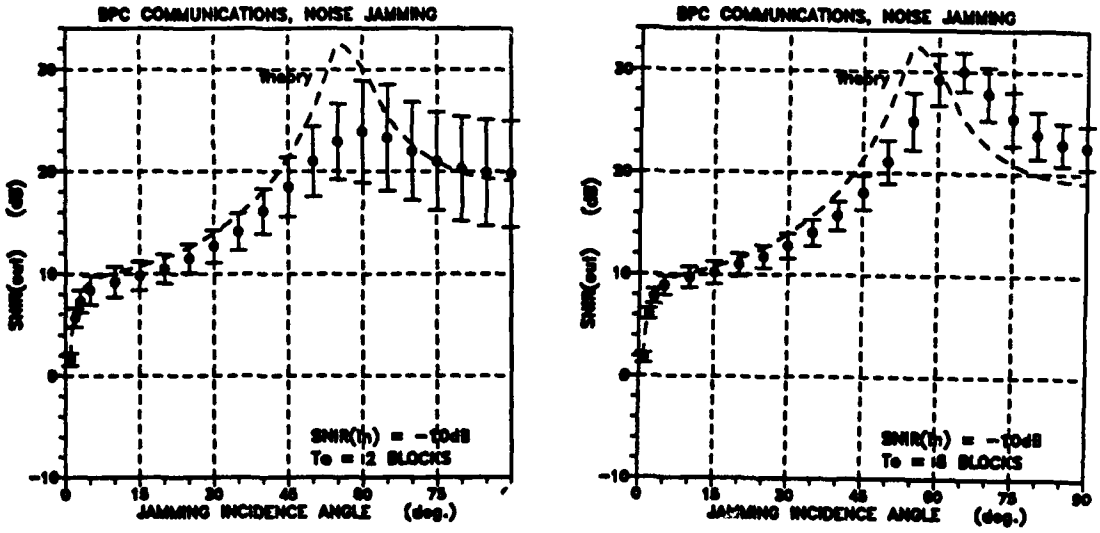

Figure 4.1 SNIR(out) as a function of jamming incidence angle, for the EV algorithm and SIR(in) = -10 dB.

Figure 4.1 shows the resultant performance in terms of SNIR(out) as a function of jamming incidence angle, for SIR(in) = -10 dB, and T_0 = 2 and 8 blocks. Both the mean values

and the rms deviations in the block estimate are plotted. Also shown on these plots are the theoretical curves computed from the expected mean covariance matrix for these conditions. (The method is described in [2].)

Under these conditions the PRI algorithm was shown to have a performance SNIR(out) of 10 dB, except for jamming directions very close to that of the communications (See Section 3.5.2, Figure 3.2). As can be seen in Figure 4.1, the EV performance improves as the jamming direction moves away from that of the communications (0° incidence), SNIR(out) remaining near the PRI result of 10 dB at angles near 0 (5-20° region) but increasing well above the PRI result at greater angles. A maximum is achieved in the 55-60° region, which is where the input signal vector from the array, due to the communications, is orthogonal to that due to the jamming. The observed result in the mean is generally lower that the theoretical result, for the shorter averaging times (T_0 = 1, 2 blocks). For the longer averaging times, the mean performance actually increases above the theoretical result at angles greater than 60°, with SNIR(out) as a function of direction being similar to that expected for a slightly smaller spacing of the elements. The differences between the observed values and theoretical values are small, relative to the improvement over the PRI performance for all values except several points in the the vicinitiy of the peak. As expected, the rms deviation in the simulation results becomes less as the averaging time constant is increased.

Figure 4.2 shows the corresponding result, for SIR(in) = -3 dB. The PRI performance for this situation does not exceed SNIR(out) = 3 dB, which for most communications signals is inadequate. SNIR(out) > 8 dB corresponds to acceptable performance for most communications signals. The EV performance is seen to exceed SNIR(out) = 8 dB, for angles > 45°. In this case, the simulated performance, in the mean, lies quite close to the theoretical performance. The rms variation in SNIR(out) decreases as the averaging time constant is increased, with the dependence on direction becoming similar to that expected for a slightly smaller element spacing.

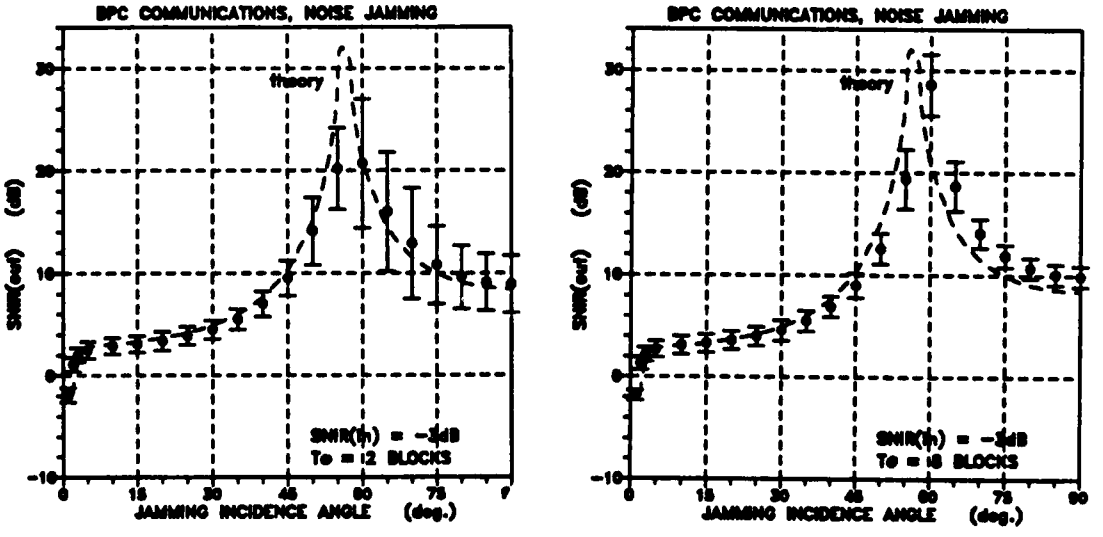

Figure 4.2 SNIR(out) as a function of jamming incidence angle, for the EV algorithm and SIR(in) = -3 dB.

4.5.2. Performance Against Time-Varying Jamming

The effect of time-varying signals on EV algorithm performance was studied, just as for the PRI algorithm, by introducing a pulsed-noise jamming signal of 50% duty cycle and 16 blocks period, at an incidence angle of 45°. As before, a mean input signal-to-interference ratio SIR(in) of -10 dB was used, and the input signal to noise ratio SNR(in) was 20 dB. Five different averaging time constants were tried, of T_0 = 1, 2, 4, 8, and 16 blocks. The simulation duration was 4096 samples, covering several cycles of pulsed jamming.

Figures 4.3a and b show the resulting performance as a function of time. Figure 4.3a shows the performance in terms of SNIR(out), for the various averaging time constants. The corresponding phase shift introduced by the array on the communications signal is plotted in Figure 4.3b; variations in this phase shift are a measure of the unwanted modulation introduced on the communications by a time-varying jamming signal. In both figures, the on-off times for the pulsed jamming are indicated.

The EV performance in the presence of pulsed jamming is affected by two mechanisms, similar in some ways to the PRI performance.

First, it is important to note that in evaluating performance, it was assumed that the second output channel had been selected as containing the communications, and that there was no means of changing channels from block to block. Provided that the jamming is the stronger signal, this will be the case. When only the communications and noise are present, the algorithm will tend to place the communications in the first channel, leaving only noise in the second channel. Thus, for pulsed jamming, the communications signal will be cancelled during the jamming-off times, in the absence of any averaging. When time-averaging is introduced in computing the weights, however, the signal separation will be based on past signals which include the previously-on jamming. Thus, provided the averaging time constant is sufficiently large relative to the jamming off-time, or the mean jamming power is sufficiently stronger than the communications, the communications will remain in the second output channel during jamming-off times.

Second, when the averaging time constant is less than the jamming off-time, the weights at the end of the off-time will be derived from only a jamming signal power much smaller than the average. This will also be the case at the beginning of the next jamming-on time, although at this time the current jamming power will exceed the average power. The degree to which the jamming signal is cancelled in the second output channel depends on how much of the jamming signal has been used in deriving the weights. Thus, even when the communications signal remains in the second output channel, there will be a tendency for the performance to drop at the beginning of the jamming-on period, for shorter averaging times.

These two mechanisms are evident in Figure 4.3a. For the shortest averaging time T_0 (1 block), SNIR(out) becomes negative towards the end of the jamming-off time. This is indicative of a change in the output channel containing the communications. (In [2] it is shown that for two signals, the ratio of output signal powers is inverted between the first and second channel. Thus when SIR(out) and thus SNIR(out) is negative for the second channel, the first channel will have a positive SIR(out), i.e., the communications has been separated into the first

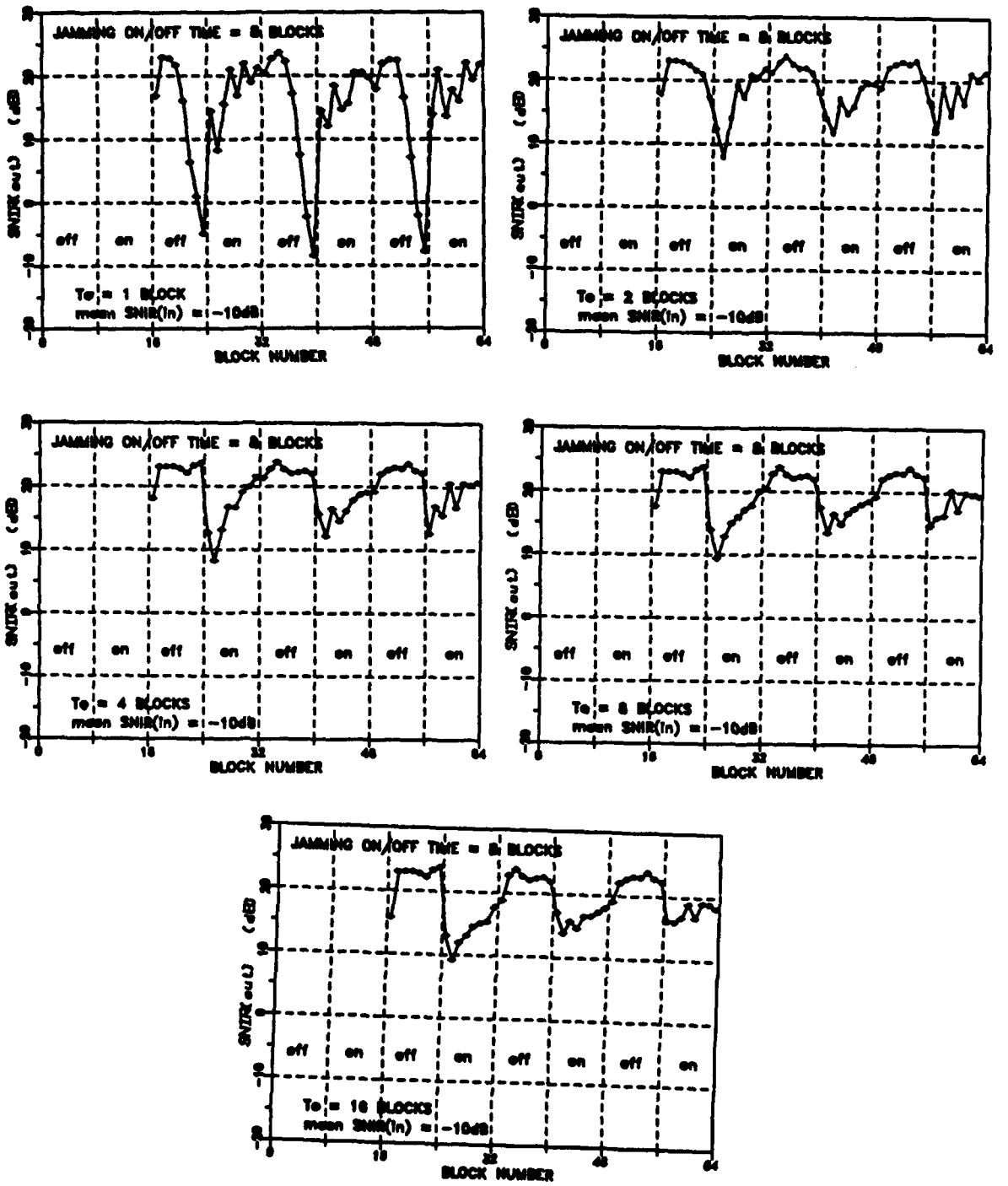

Figure 4.3a Performance of the 2-element EV adaptive array algorithm, against pulsed-noise jamming, in terms of SNIR(out) as a function of time, for various averaging time constants.

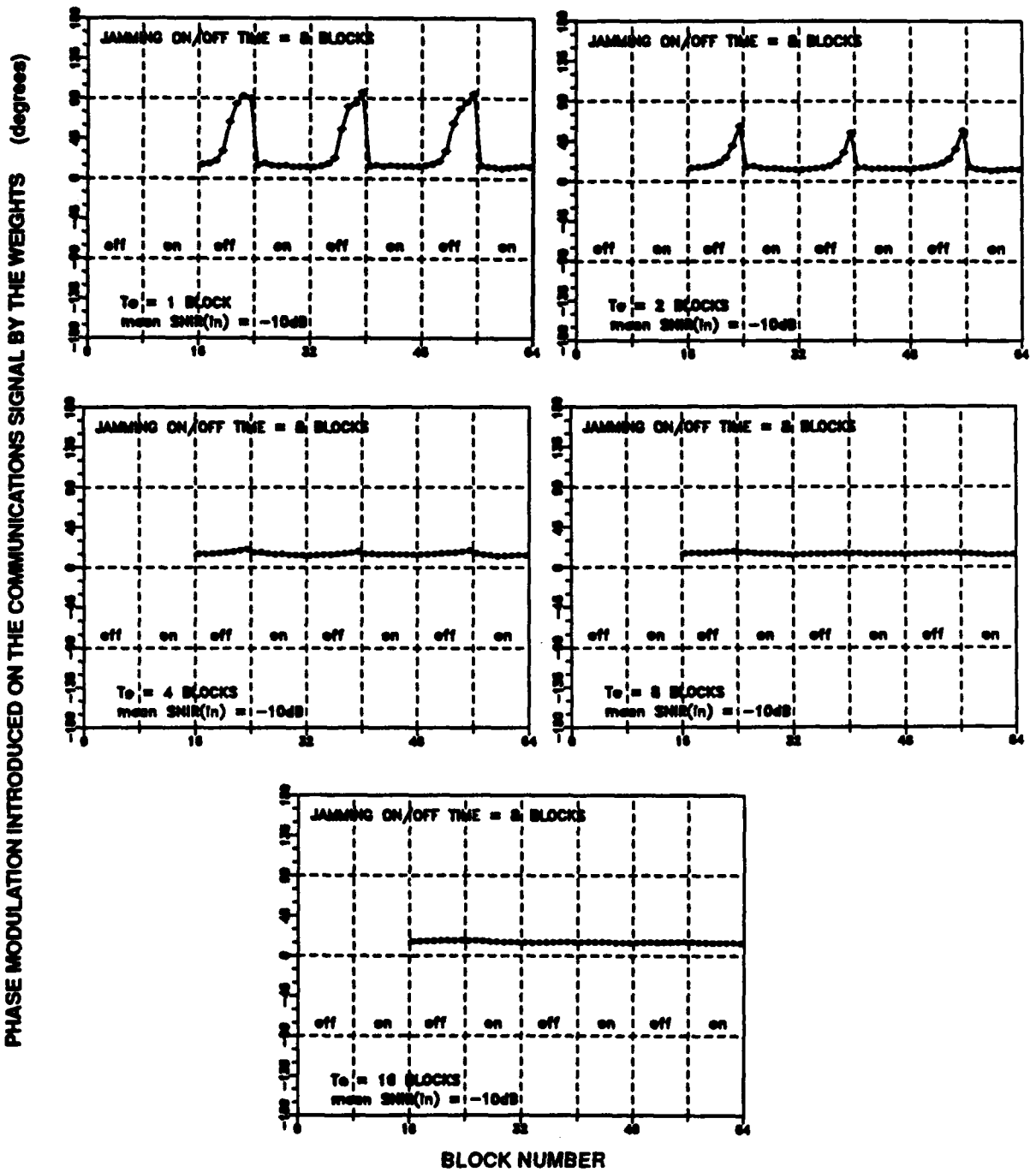

Figure 4.3b Performance of the 2-element EV adaptive array algorithm, against pulsed-noise jamming, in terms of the phase modulation introduced by the weights on the communications signal as a function of time, for various averaging time constants.

channel rather than the second channel.) For a slightly longer averaging time T_0 (2 blocks), SNIR(out) remains positive throughout the jamming-off times, indicating that the second output channel continues to contain the communications signal. For this averaging time, the performance is worst at the onset of the jamming-on time, as expected on the basis of the second effect noted above. As the averaging time is increased, from 2 to 16 blocks, the minimum performance becomes increasingly better.

A comparison of the EV results of Figure 4.3a with those for the PRI algorithm (Section 3.5.3, Figure 3.3a) is useful. The EV algorithm performs better for lower averaging times. For example, at $T_0 = 2$ blocks, with the EV algorithm, SNIR(out) has a minimum value in excess of 8 dB, while with the PRI algorithm SNIR(out) drops as low as -12 dB. The averaging time employed will be a compromise between that required to handle time-varying signal powers, and the fast response needed to deal with changes in signal direction. From this comparison it appears that the EV technique may be better in handling such a compromise.

Figure 4.3b reveals another facet of EV performance. The phase response of the array to the communications signal is affected by the pulsed jamming. This effect is quite strong for the shortest averaging time T_0 (1 block), with 90° swings in the output phase occurring near the end of the jamming-off times. At the next averaging time T_0 (2 blocks), phase modulation still occurs, but is at a more acceptable level, near 45°. At the longer averaging times, it is negligible.

The phase modulation is not quite as severe with the PRI algorithm. A comparison of the EV and PRI phase response for $T_0 = 2$ blocks shows less modulation with the PRI algorithm than with the EV algorithm. The 45° modulation noted with EV is near the maximum acceptable value for binary-phase-coded signals. For quadrature or higher-order phase codes, it is not acceptable.

4.6 SIMULATION FINDINGS

The results with simulated signals indicate significant improvements in performance with the EV algorithm, over the PRI algorithm, approaching those predicted by theory. This improvement is reflected both against constant-power signals, and time-varying signals. In the case of time-varying signals, the EV algorithm does not need nearly as long an averaging time constant to avoid communications cancellation. However, a slightly longer averaging time is needed with the EV algorithm to avoid phase modulation effects caused by time-varying interference. Since the averaging time is a compromise between being long enough to fill in the jamming-off or interference-fade times, and being short enough to respond to changes in signal directions or antenna orientations, the EV algorithm may be better suited to changing conditions.

The EV algorithm implemented here includes input-channel power normalization, which is an attempt to provide equal channel gains. A previous study [2] showed the EV algorithm attains its best performance when the gains are equal. In practice, the antennas themselves will have different, direction-dependent gains, making such compensation impossible. The simulated signals do not take such antenna differences into account, nor are these differences well-known. Therefore it is necessary to use real-world signals in order to properly characterize the EV algorithm performance under operational conditions.

5.0 SYSTEM PERFORMANCE MEASUREMENTS

5.1 LIMITS TO NULL DEPTH

5.1.1 Differential Frequency Response of the Input Channels

The most significant limitation to the processing gain, or null depth achievable against interference, in a narrowband adaptive antenna system is the differential frequency response of the receivers. Because of the differential frequency response, each frequency component of the interference has a phase and amplitude input channel dependence that is different from other frequency components. The weights needed to cancel one frequency component will not cancel the other frequency components, in general. The interference cancellation is limited by the degree of mismatch that exists between the input channels across the bandwidth of the received interference.

It can be shown that the null depth limit, expressed as the ratio of the optimally adapted array response δP (power) for the interfering signal, to the mean response $\bar{P}$ over all input directions for a signal of similar strength, is given by

$$\left(\frac{\delta P}{\bar{P}}\right)_f = \overline{(\delta\theta)^2} + \overline{\left(\frac{\delta A}{\bar{A}}\right)^2} \qquad (5.1)$$

where $\overline{(\delta\theta)^2}$ is the mean-square difference from the mean, in the phase response difference between channels over all frequencies, expressed in radians; and $\overline{\left(\frac{\delta A}{\bar{A}}\right)^2}$ is the corresponding mean-square difference from the mean, in the amplitude response difference between channels expressed as a fraction of the mean amplitude response for that channel. For most systems the rms differences arise mainly in the final-stage filters, which set the maximum bandwidth for the interference seen by the weights. Equation 5.1 assumes the weights are optimum, and not affected by noise fluctuations in the signals.

The null depth limit arising from the differential frequency response was determined by measuring the phase and amplitude response of the input channels at a number of baseband frequencies uniformly spaced across the receive bandwidth. From these responses, the mean difference in phase and amplitude response between each pair of channels over the measured frequencies was obtained, along with the mean-square difference from the mean. The mean-square differences were then averaged over all channel pairs, to obtain $\overline{(\delta\theta)^2}$ and $\overline{\left(\frac{\delta A}{\bar{A}}\right)^2}$.

The measurement arrangement is shown in Figure 5.1. A frequency synthesizer, set to an RF frequency of 50 MHz plus the baseband frequency f, provided the input signal. this signal was split and fed to the two receivers of the adaptive antenna system which were coherently tuned to 50 MHz. In the adaptive antenna receiving system, the IF outputs of the receivers are fed to the I/Q demodulator which reduces the two input signals to pairs of in-phase (I) and quadrature (Q)

signals. These four signals are passed through matched analog low-pass filters and fed to the programmable processing system. For the differential response measurements, the processing system was run with fixed weights, set equal to one of (1, 0, 0, 0) , (0, 1, 0, 0) , (0, 0, 1, 0) , or (0, 0, 0, 1), to pass the channel 1, 2, 3, or 4 signal, respectively, to the output. The output signal was filtered to remove the D/A conversion noise and then fed to an amplitude/phase meter. The channel-1 input signal was tapped and fed to the meter, as a phase reference.

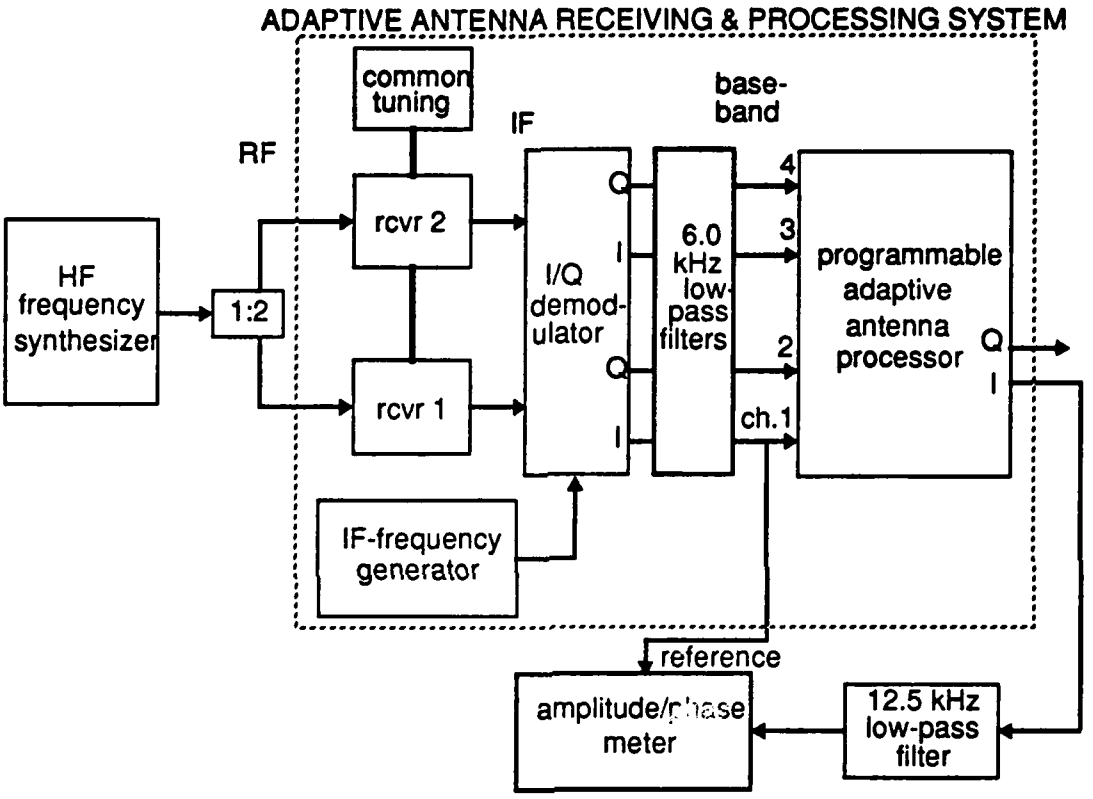

Figure 5.1. Frequency response measurement arrangement.

The resulting fractional amplitude differences from the mean, found for each of the channels, are plotted as a function of baseband frequency f in Figure 5.2a. The corresponding phase differences between channels 2, 3, 4, and channel 1 are plotted in Figure 5.2b, along with the mean values. The mean-square deviations in these quantities are:

$$\overline{(\delta\theta)^2} = 3.316 \times 10^{-4} \text{ (radians)}^2$$

$$\overline{\left(\frac{\delta A}{\bar{A}}\right)^2} = 2.110 \times 10^{-4}$$

From equation (5.1), the corresponding null depth limit is 2.99×10^{-4}, or -35 dB.

Similar tests were made using a cutoff frequency of 12.5 kHz for the precision low-pass filters. The null-depth limit across this wider bandwidth was also found to be -35 dB. This is not

surprising when one considers that mismatches between the precision low-pass filters which define the signal bandwidth are the main source of the differential frequency response. Provided that the component mismatches are similar, for the components selected for the different bandwidths, the effect on null depth should be independent of the bandwidth selected.

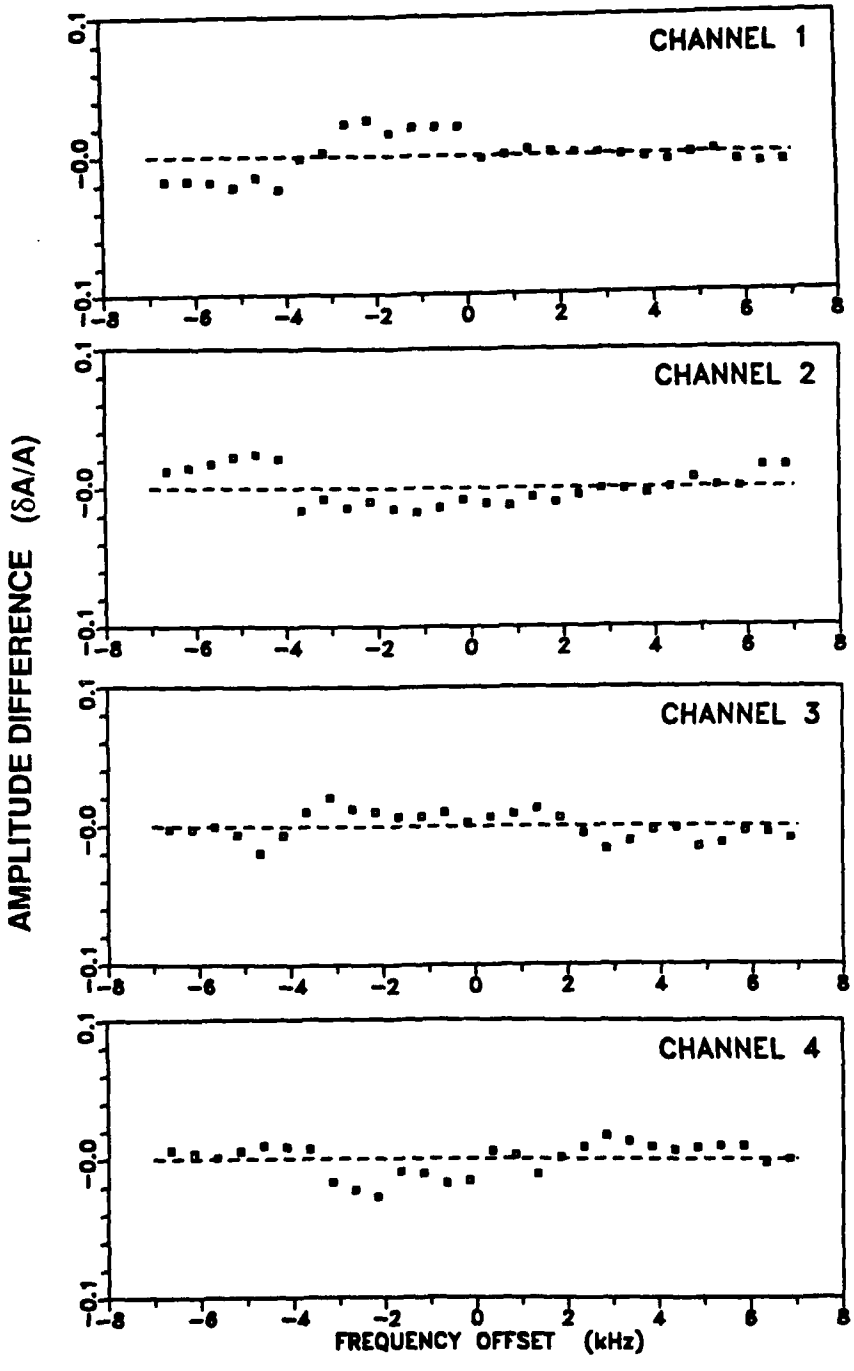

Figure 5.2a. Difference from the mean, in the channel amplitude response, as a function of baseband frequency, for the four input channels.

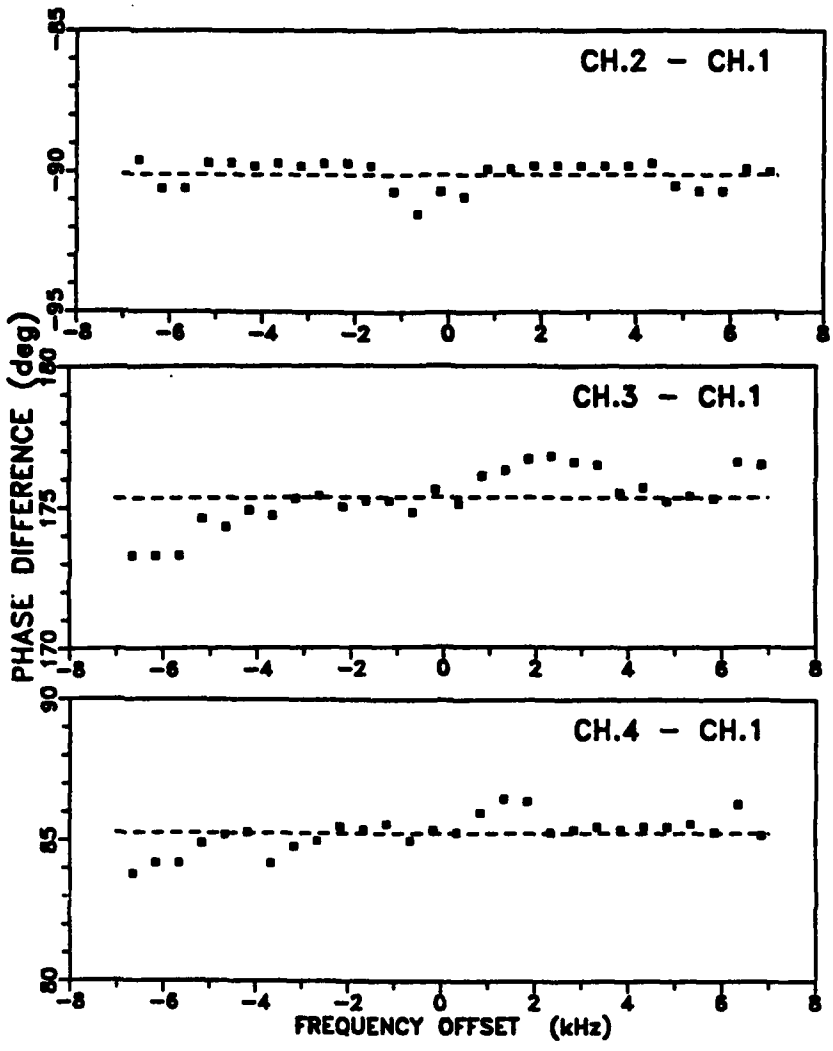

Figure 5.2b. Phase Response differences between channels, as a function of baseband frequency

5.1.2 Receiver Phase Noise

No oscillator is perfectly stable. This includes the frequency-synthesized local oscillators of the WJ-8628A-1 receivers used in the adaptive antenna processing system. The random phase fluctuations of the local oscillators are added to the received signal, in the frequency downconversion process. As phase coherence between receivers is maintained in the present system by the sharing of a common frequency standard rather than by using common local oscillators, these random phase fluctuations differ between receivers, and appear in the relative phase of signals as seen by different receivers. As a result, a set of weights that is constant over the time scale of the fluctuations will not be able to cancel a phase-fluctuating interference signal perfectly.

The null-depth equation (5.1) can be adapted to this problem, by treating the receiver phase fluctuations as frequency-dependent phase variations between channels, and ignoring any amplitude fluctuations. The minimum null depth (expressed as a power δP relative to the mean

power $\bar{P}$ over all directions) set by the phase noise then becomes

$$\left(\frac{\delta P}{\bar{P}}\right)_p = \overline{(\delta\theta)^2} \tag{5.2}$$

where $\overline{(\delta\theta)^2}$ is the mean-square phase fluctuation introduced by each of the receivers.

The receiver-introduced phase fluctuations are manifested in the receiver sideband noise. A phase fluctuation of $\delta\theta$ and modulating frequency f_m will lead to two noise components, each of amplitude $(V\delta\theta)/2$ where V is the amplitude of the signal being received, and having frequencies $\pm f_m$ relative to that of the signal [5]. The resulting mean-square phase fluctuation is given by the normalized noise power P_n/P_s integrated over the positive and negative sidebands, where P_s is the signal power, so that the associated null depth limit is given by

$$\left(\frac{\delta P}{\bar{P}}\right)_p = \frac{P_n}{P_s} . \tag{5.3}$$

From the data sheets for the WJ-8628 receiver, the normalized noise power over the sideband range 100 Hz (the fastest response frequency for the weights with the algorithm parameters normally chosen in testing) to 12.5 kHz (the lowpass filter cutoff normally used) was determined to be -48 dB. A factor-of-two change in either of these limits produces less than 1 dB change in this value. Thus, the receiver phase noise can be said to limit the null depths achievable by the present system to -48 dB.

5.1.3 Digital Processing Precision

The A/D conversion places a limit on the null depths achievable by the system, as a result of the quantization noise which is added to the input samples upon conversion. As the weights are derived from the samples, the null depth is, in general, dependent on the adaptation algorithm and its parameters. However, if we can assume that sufficient averaging is employed in the weight calculation to make the errors on the weights negligible, the null depth limit due to quantization can be shown to be given by

$$\left(\frac{\delta P}{\bar{P}}\right)_q = \frac{(\delta V)^2}{3\overline{V^2}} \tag{5.4}$$

where δV is the A/D conversion precision (one-half bit, neglecting offset errors) and $\overline{V^2}$ is the mean-square input signal voltage presented to the A/D converters (channel-independent by assumption). The present system employs 12-bit (11 bits plus sign) A/D converters. The channel gains were adjusted so that the maximum signal was near half-scale and that the rms signal $\sqrt{(\overline{V^2})}$ was typically 9 bits long. Assuming that the weights are set primarily by the stronger (jamming) signal, the array gain for the wanted signal, on average, will be unity. Under these conditions, equation (5.2) results in a null depth limit near -65 dB. This neglects any offset errors that the A/D converters may have. A realistic maximum A/D offset error is of the order of 2 bits. Under these conditions, equation (5.2) predicts a null depth limit as high as -47 dB (of the same order as the receiver phase noise limit).

5.1.4 Total Null Depth Limit and Corresponding Maximum Processing Gain

The total null depth limit due to the various effects represented by equations (5.1), (5.3), and (5.4) (differential frequency response, receiver phase noise and quantization noise) is merely the sum of the separate limits:

$$\left(\frac{\delta P}{P}\right) = \left(\frac{\delta P}{P}\right)_f + \left(\frac{\delta P}{P}\right)_p + \left(\frac{\delta P}{P}\right)_q . \qquad (5.5)$$

If g_s is the voltage gain of the array toward the wanted signal, relative to isotropic, the corresponding maximum processing gain is given in terms of the null depth limit, by

$$G_{max} = (g_s)^2 \left(\frac{\delta P}{P}\right)^{-1} . \qquad (5.6)$$

For pure-tone jamming signals the null depth limit will be that imposed by the receiver phase noise and the quantization noise, and will lie somewhere between -48 and -45 dB. For full-bandwidth jamming signals such as white-noise, the null depth will be limited primarily by the differential frequency response to a minimum of -35 dB.

5.2 TESTS WITH IN-LAB SIGNALS

The adaptive-antenna system was evaluated using laboratory-generated signals, together with an RF distribution system that simulated a desired signal and a jamming signal arriving on an array from various directions. The distribution system is shown schematically in Figure 5.3.

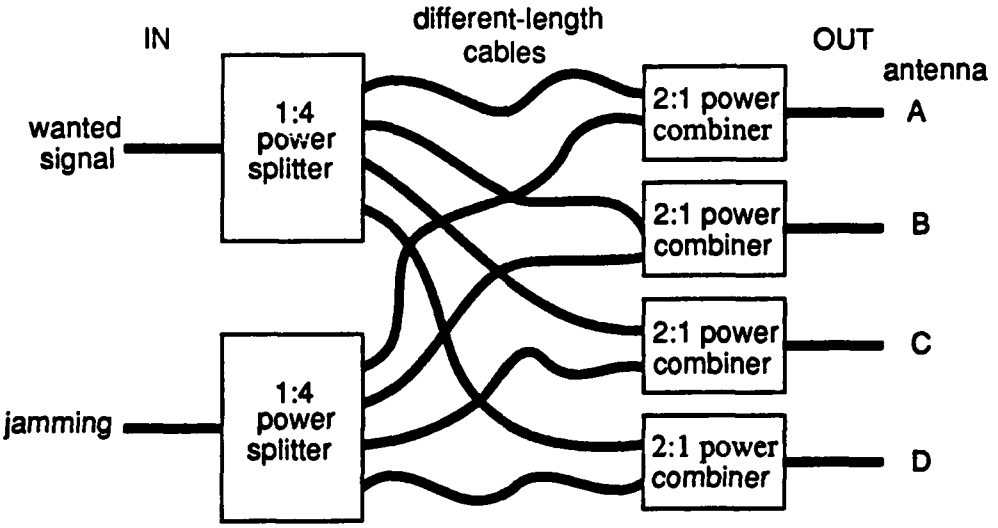

Figure 5.3 In-lab RF signal distribution system

The desired signal is split four ways, passed through cables of selected different lengths into power combiners, where the signal is combined with the similarly treated jamming signal. The cable lengths are selected appropriately for the desired signal and the jamming, so that the signals at the output of the distribution system look like the signals received by an antenna array of a given geometry, with desired and jamming incident from different specific directions. The

distribution system permits different cable lengths to be switched in, chosen so that the array appears as four elements at the corners of a 2-meter square, with the desired and jamming signals each incident from 0°, 10°, 30° or 90° relative to one side of the square. The simulated array geometry and allowed signal directions are illustrated in Figure 5.4.

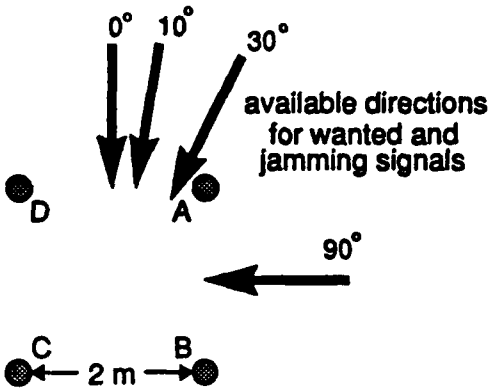

Figure 5.4 Array geometry and signal directions simulated by signal distribution system.

The operating arrangement used for the tests with in-lab signals is shown in Figure 5.5. Specifically generated RF wanted and jamming signals are fed to the distribution system. Two of the distribution-system outputs are then fed to two receivers of the adaptive-antenna system. The wanted signal cabling was set to the 0° direction (Figure 5.4), and the jamming signal cabling to one of the other three directions. The outputs selected were either A and D, or A and B (Figure 5.4), corresponding to broadside or endfire. For the tests, the precision low-pass filters were set to either a 6.0-kHz cutoff (for FSK wanted signals) or 12.5-kHz cutoff (for all other cases).

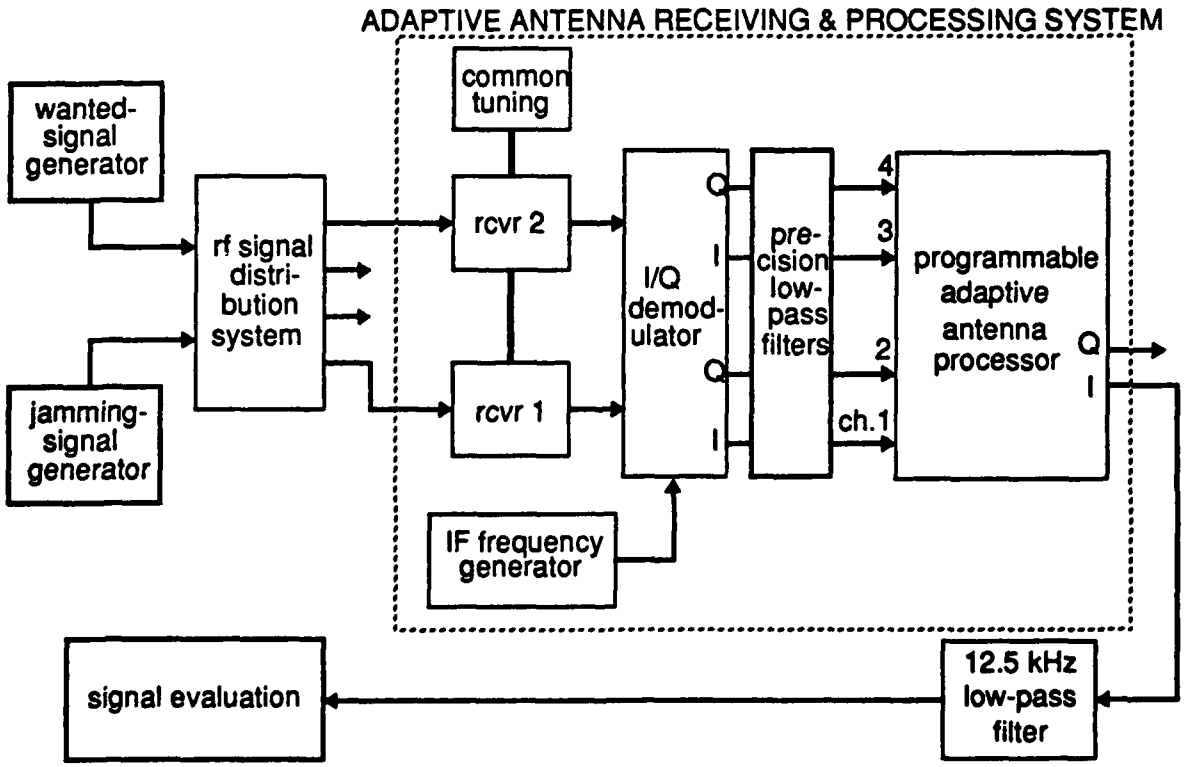

Figure 5.5 Equipment configuration for tests with in-lab signals.

5.2.1 Pure-Tone Signals

Initial operating tests of the system used the PRI and EV algorithms and pure-tone wanted and jamming signals. As the (zero) bandwidth of the signals was substantially less than the effective RF bandwidth set by the low-pass filters (25 kHz, corresponding to 12.5-kHz cutoff), the processing gain or null depth limit was expected to be set by the A/D conversion accuracy and receiver phase noise rather than the differential frequency response of the channels. Test parameters are given in Table 5.1. As previously discussed, the input signal levels were set to roughly half the input range of the A/D converters.

Table 5.1 Parameters used in pure-tone signal tests

RF frequency	50 MHz
wanted signal	700-Hz pure tone, incident broadside
jamming signal	4.0-kHz pure-tone, incident 10°, 30°, and 90° relative to broadside
receive bandwidth	25 kHz
I/Q sampling rate	40 kHz
algorithm parameters	50-sample block length (2 ms), 5-block averaging time constant (10 ms)

The input signal levels were found by replacing the adaptation algorithm with fixed weights selected so as to pass the signal incident on a single antenna without change, then turning on either the wanted or jamming signal by itself and measuring the signal power at the output of the processing system. The output signal levels were found by running the adaptation algorithm with both wanted and jamming signals present, then freezing the weights and measuring the output signal power with only one signal (wanted or jamming) present at a time.

The results obtained with the PRI algorithm are shown in Figures 5.6a and b.

Figure 5.6a shows the output signal-to-interference ratio SIR(out) in dB, as a function of the input ratio SIR(in). The expected power inversion performance is also shown as a straight line of slope -1. Results are plotted for the three jamming directions tested. As can be seen, the observed performance agrees with that expected for the higher input signal-to-interference ratios SIR(in). At some point As SIR(in) is decreased, the performance begins to fall short of the expected result. This happens sooner for smaller angular separations between wanted signal and jammer. A comparison with the corresponding simulated-signal result (Figure 3.1) is revealing of the cause. The simulated-signal performance began to fall short of the theory when the expected SNIR(out) became limited by input noise. As the simulated signal noise was set constant relative to the communications. and input noise is not reduced at the output, a fixed upper limit was reached for SNIR(out). In the present real-signal case, the hardware introduced two 'noise' sources that were proportional to the total signal: receiver phase noise and quantization noise. As SIR(in) is decreased this noise becomes proportionately higher relative to the wanted signal, i.e., SNR decreases. Thus, as SIR(in) is decreased past where this noise first limits SNIR(out), SNIR(out) begins to decrease proportional to SIR(in). This is seen in Figure 5.6a.

Figure 5.6b shows the same results expressed in terms of processing gain G. As SIR(in) is decreased, G increases in a manner consistent with the theoretical prediction up to a limiting value which depends on angular separation. Beyond this point, G becomes constant, consistent with the hardware-limitations to performance described in the previous paragraph. From this figure, the limiting values for G are 24, 32 and 47 dB, for jamming directions of 10°, 30° and 90°.

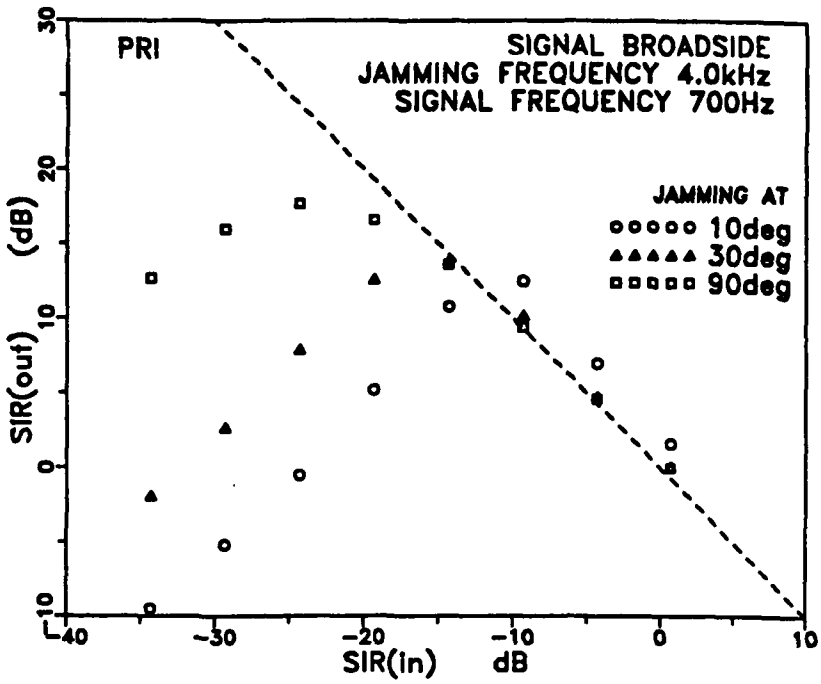

Figure 5.6a SIR(out) as a function of SIR(in), for a pure-tone wanted signal at broadside incidence, and a pure-tone jamming signal, incident at 10°, 30°, and 90° relative to broadside, using the PRI algorithm.

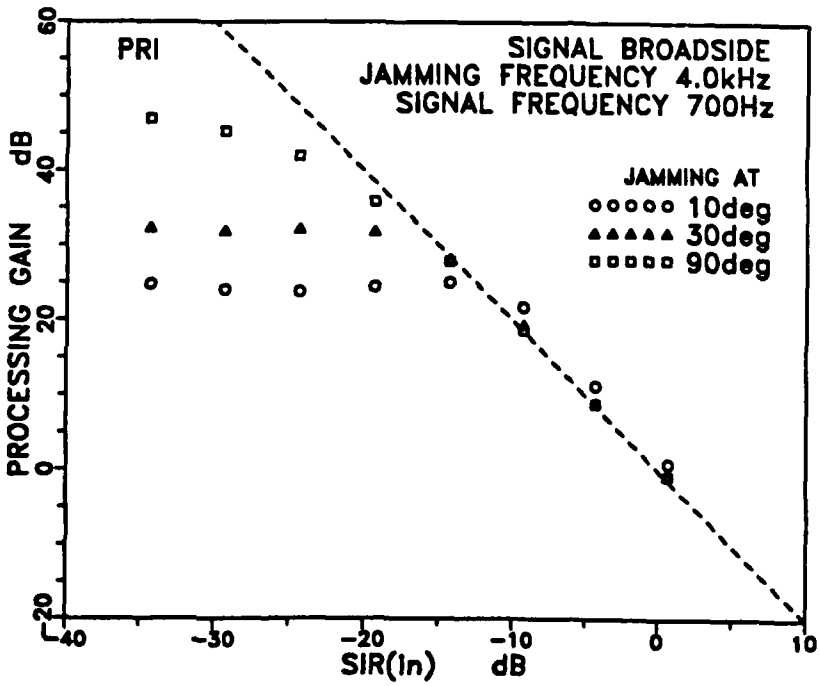

Figure 5.6b Processing gain as a function of SIR(in), for a pure-tone wanted signal incident broadside, and a pure-tone jamming signal, incident at 10°, 30°, and 90° relative to broadside, using the PRI algorithm.

From the geometry and RF frequency involved, the estimated gains g_s in the wanted-signal direction with the array null steered in the jamming direction (as it will be for very low input ratios SIR(in)), are -11.9, -3.0, and +1.8 dB relative to isotropic, for jamming directions 10°, 30°, and 90°, respectively. Using these figures together with the observed limiting values for G in equation (5.5) results in equivalent null depths of -36, -35, and -45 dB, respectively. Most of these null depths are above those expected on the basis of quantization and receiver phase noise on the samples alone (-48 to -45 dB). This implies that the assumption of optimum weights is incorrect and that quantization and receiver-phase-noise errors, as well as merely affecting the samples, also affect the estimated weights (which are dependent on signal direction) so as to limit the null depth more when the signals are close in direction.

Figure 5.7 shows the corresponding processing gains achieved with the EV algorithm, for pure-tone signals. The gains appear limited for very low values of SIR(in), to values of 22, 29, and 48 dB, corresponding to jamming incident at 10°, 30°, and 90° respectively. The corresponding null depths are -34, -32, and 46 dB, respectively. The shallow null depths found for the 10° and 30° incident jamming suggest that the weights found with the EV algorithm were significantly affected by receiver-phase and quantization noise, at least for the two cases where the signals were relatively close in direction.

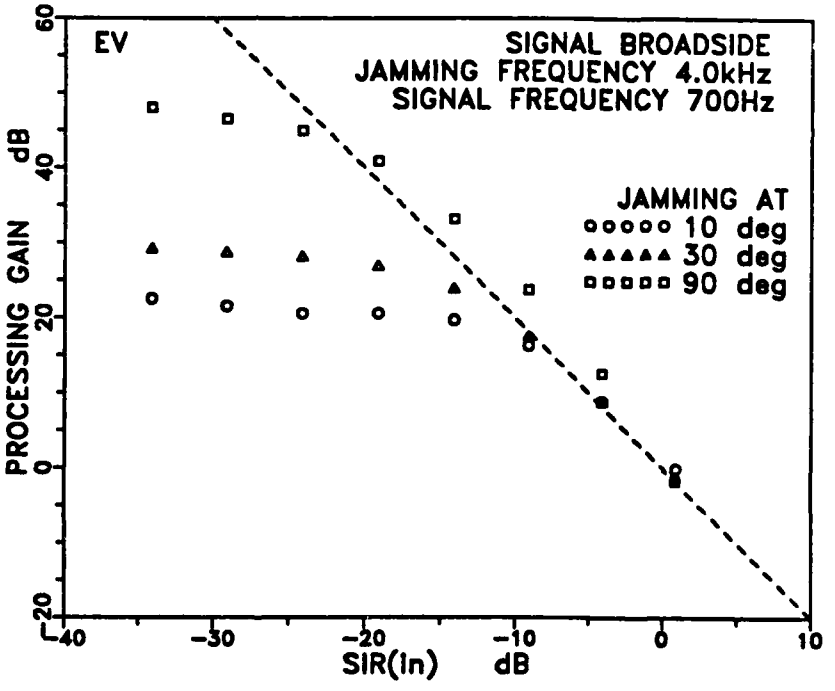

Figure 5.7 Processing gain as a function of SIR(in), for a pure-tone wanted signal incident broadside, and a pure-tone jamming signal, incident at 10°, 30°, and 90° relative to broadside, using the EV algorithm.

The corresponding theoretical power inversion performance is also shown on Figure 5.7, as a dotted line. At the higher values of SIR(in), before limiting is approached, the processing gain achieved with the EV algorithm for the largest signal separation (90°) is higher than that of power inversion, by 5 or 6 dB typically. This is in contrast to the PRI performance shown in Figure 5.6b, where the performance is close to that of power inversion.

In summary, the array performance is limited by the receiver phase noise and quantization

to null depths no deeper than -48 to -45 dB, for both the PRI and EV algorithms. When the incoming signals are close in direction, these signal-related noise effects also affect the weights, limiting the null depths yet further. The EV algorithm is observed to have a better performance than the PRI algorithm for large signal separations, when the input jamming signal is not so much stronger than the wanted signal that the performance is reduced by the null-depth limit.

5.2.2 Noise Jamming and Pure-Tone Wanted Signal

The system performance was characterized in terms of processing gain G, for both the PRI and EV algorithms, using a pure-tone wanted signal, and a white-noise jamming signal. The parameters for these measurements are listed in Table 5.2.

Table 5.2 Parameters used in white-noise jamming/ pure-tone wanted-signal tests

RF frequencies	35, 50 and 80 MHz
wanted signal	4.0-kHz pure-tone, incident broadside and endfire
jamming signal	white-noise, incident 10°, 30°, and 90° relative to broadside
receive bandwidth	25 kHz
I/Q sampling rate	40 kHz
algorithm parameters	50-sample block length (2 ms), 5-block averaging time constant (10 ms)

Several RF frequencies spanning the VHF land-mobile band were employed, along with various wanted-signal and jamming-signal directions. Other parameters were similar to the pure-tone tests of the previous section.

The feature of the input signals that permits their separation by an adaptive array is the phase difference between antennas, which is a function of the input direction, RF frequency, and array geometry. The differences between the two simulated antennas (Figure 5.4) in terms of the relative phases of the desired and jamming signals, for the in-lab operating frequencies and simulated signal directions, is shown in Table 5.3. The ability of a system to separate signals depends directly upon this relative difference.

Table 5.3 Relative difference in phase between antennas, for the signal directions and RF frequencies used.

wanted-signal direction		endfire		broadside		
jamming direction		10°	30°	10°	30°	90°
RF frequency	35 MHz	1.3°	11.2°	14.6°	42.0°	84.0°
	50 MHz	1.8°	16.1°	20.8°	60.0°	120.0°
	80 MHz	2.9°	25.7°	33.3°	96.0°	192.0°

5.2.2.1 PRI Algorithm

Figure 5.8 shows the processing gains achieved with the PRI algorithm as a function of input signal-to-jamming ratio SIR(in), at the three RF frequencies, for a broadside wanted signal and a jamming signal incident at 10°, 30°, and 90°.

Similar to the previous result with pure-tone signals, the PRI algorithm performance is seen in Figure 5.8 to be that of power inversion, for SIR(in) between 0 and -15 dB. The processing gain varies as the inverse square of SIR(in) over this range. At lower values, the processing gain reaches an asymptotic limit that depends somewhat on the RF frequency and input signal directions, being higher for the higher RF frequencies and greater azimuthal signal separations. The largest gains achieved are approximately 32 dB, somewhat lower than the 47 dB achieved for the pure-tone signals. The limited processing gain against the finite-bandwidth white-noise jamming is set by the differential frequency response of the receivers, which, on the basis of measurements was seen to be 35 dB (Section 5.1.1).

A clearer picture of the performance variation may be gained by plotting the adaptive array performance against the relative phase difference between antennas, of the wanted and jamming signals. Figure 5.9 shows SIR(out) obtained for a specific SIR(in) with the PRI algorithm, as a function of the relative phase difference. The phase differences are given in Table 5.3 for the various signal directions and RF frequencies used. Figure 5.9 contains three plots, corresponding to SIR(in) of -5, -10, and -20 dB respectively. Also shown on these plots is a dashed line, representing the performance expected on the basis of power inversion.

For SIR(in) = -5 and -10 dB, the performance is seen in Figure 5.9 to be close to that of power inversion, for all but the smallest (<15°) relative phase differences. At SIR(in) = -20 dB, the performance falls short of power inversion by roughly 10 dB. This is due to the limited gain against finite-bandwidth signals caused by the differential channel frequency response described above, which requires SIR(out) to be at least 5 dB below power inversion in this case.

When the relative phase differences are small, performance is reduced. This condition corresponds to the wanted and jamming signal directionss approaching each other, and reflects the inability of the array to place a null in the direction of the stronger (jamming) signal without also cancelling most of the wanted signal. As described in Section 3.5.2 for the simulated signal tests, the wanted signal is reduced while channel noise remains the same. The main contribution to channel 'noise' in the present measurements is the channel mismatch, with receiver phase noise and A/D quantization noise playing a lesser role. From Figure 5.9, when the input wanted signal is much less than the jamming signal, the reduced performance extends over greater differences in jamming/wanted signal arrival directions. This is expected, since the channel noise (consisting mainly of channel mismatch noise which depends on total input signal power) has not changed.

In summary, these tests of the adaptive array with the PRI algorithm indicate that the performance is close to power inversion, except for very small SIR(in) where the expected power inversion gain exceeds the gain limitations imposed by the differential frequency response of the input channels, and for small relative phase differences where the nearly equal signal directions result in wanted-signal cancellation.

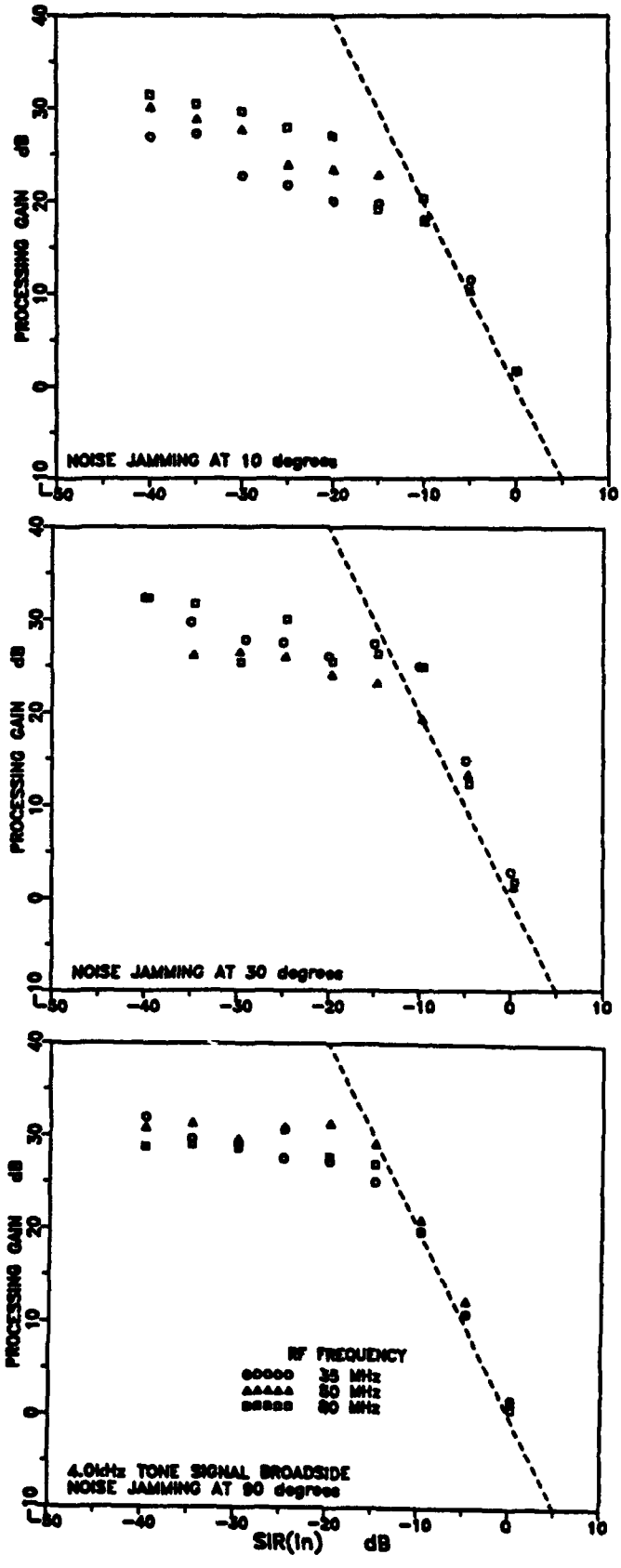

Figure 5.8 Processing gain attained by the PRI algorithm, against white noise jamming, as a function of SIR(in), for 3 RF frequencies and 3 different jamming directions.

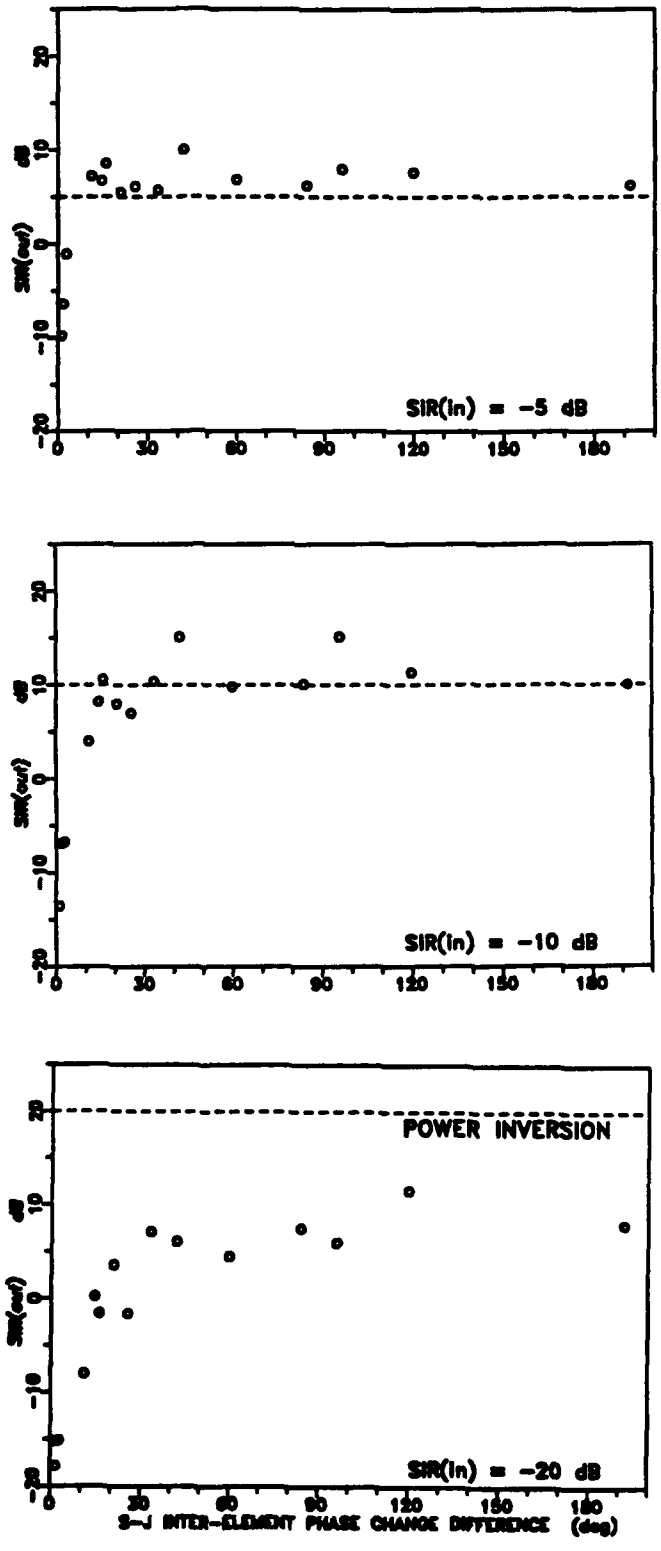

Figure 5.9 SIR(out) as a function of the difference between antennas, in the relative phase of the wanted and jamming signals, for the PRI algorithm against white-noise jamming, for various levels of SIR(in).

5.2.2.2 EV Algorithm

The measurement results for the EV algorithm are shown in Figure 5.10. This figure displays the processing gain achieved using the EV algorithm with a broadside pure-tone wanted signal and white noise jamming, as a function of SIR(in), for the 35, 50 and 80 MHz RF frequencies. Separate graphs are included for jamming incident at 10°, 30°, and 90°. Also shown on these graphs are dotted straight lines representing the power inversion performance.

For the lower jamming/wanted signal direction separations (10°, 30°), Figure 5.10 displays results that are very similar to those of the PRI algorithm (Figure 5.8). The EV algorithm performance is close to that of power inversion, for SIR(in) between 0 and -15 dB, with the gain increasing as the inverse square of SIR(in), as SIR(in) decreases. Eventually the gain reaches an upper limit that depends somewhat on the RF frequency and jamming direction, but whose largest values are of the order of 35 dB, similar to the gain limit expected from the differential channel frequency response (35 dB).

At the largest jamming/wanted signal direction separation (90°), the processing gains for SIR(in) between 0 and -15 dB are considerably better than power-inversion. This is expected, as both the theory and previous simulation results indicate better performance for the EV technique when the input signals are sufficiently separated in their arrival directions. As with the lower separations, when SIR(in) drops below -15 dB, the processing gain approaches a maximum near 35 dB.

Figure 5.11 shows the corresponding performance in terms of SIR(out), plotted against the difference between antennas, in the relative phase of the wanted and jamming signals. Plots are shown in this figure for three values of SIR(in): -5, -10, and -20 dB. Included on these plots are dotted lines representing the power-inversion value, and the expected theoretical EV performance, based on an input noise level 40 dB below the jamming signal level. At the larger values of SIR(in) (-5 and -10 dB), the performance remains close to the theoretical value, with significant improvements above power inversion for relative phase changes approaching 180°. For SIR(in) of -20 dB, the performance is reduced as a result of the 35-dB processing-gain limit, to values below that of power inversion.

As for the PRI algorithm, the EV algorithm performance is reduced for small relative phase changes between antennas, where the jamming and wanted signals approach each other in direction. This effect will occur regardless of the adaptation algorithm that is used, as it is a result of the limited array aperture and the wanted signal falling inside the (resultant finite-width) receiving-pattern null centered on the jamming direction.

In summary, the EV algorithm at SIR(in) between 0 and -15 dB, behaved according to theory, with considerably better than power-inversion performance when the wanted and jamming signals were well-separated in direction. At lower SIR(in), the performance, like that of the PRI algorithm, was limited by the differential frequency response, to a maximum processing gain near 35 dB.

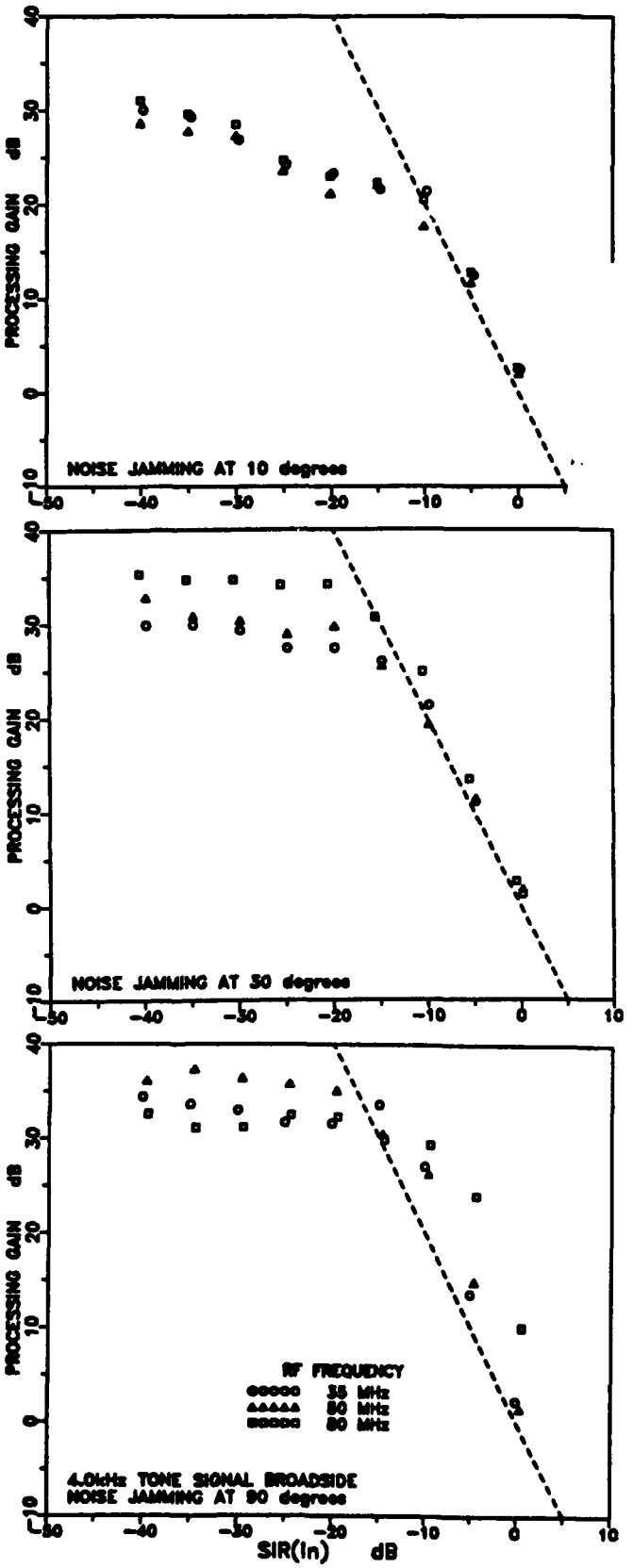

Figure 5.10 Processing gain attained by the EV algorithm, against white noise jamming, as a function of SIR(in), for 3 RF frequencies and 3 different jamming directions.

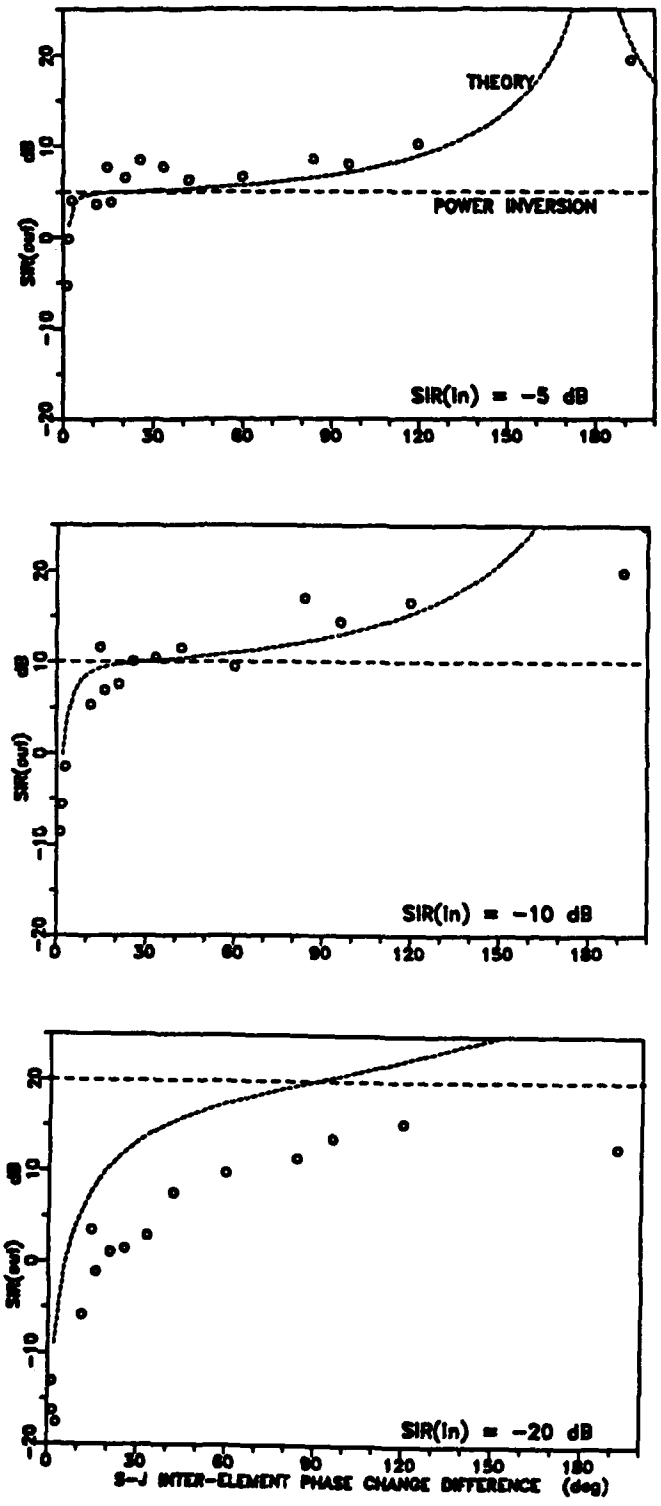

Figure 5.11 SIR(out) as a function of the difference between antennas, in the relative phase of the wanted and jamming signals, for the EV algorithm against white-noise jamming, for various levels of SIR(in).

5.2.3 FSK Wanted Signal and Noise Jamming

In any operational communications system, the output signal-to-noise-plus-interference ratio SNIR(out) is required to be above a minimum threshold value for acceptable communications. The present adaptive antenna processing system is limited by the theoretical performance of the algorithm employed at low input jamming levels, and by the differential channel frequency response at higher jamming levels. As the theoretical performance for the algorithms tested is close to that of power inversion in many instances, this places a lower limit as well as an upper limit to the range of input jamming levels over which acceptable performance will be attained.

In order to determine the useful operating range, tests were made, using a data signal in the presence of white-noise jamming. A 2.4 kB-FSK signal was used, and a predetermined message generated. This signal was converted to RF frequencies and passed through the cable network to the receiving system. The filtered output of the adaptive antenna processing system was passed to a data error analyzer, capable of recognizing and synchronizing to the predetermined message, and counting the number of bits in error. In this way, a bit error rate measurement was made, for various wanted-signal and jamming directions, RF frequencies, and values of SIR(in). Table 5.4 shows the operating parameters used in these tests.

Table 5.4 Parameters used in white-noise jamming/FSK wanted-signal tests

RF frequencies	35, 50, 65 and 80 MHz
wanted signal	2.4-kB/s FSK with 1.8 and 4.2-kHz mark and space tones, incident broadside
jamming signal	white-noise, incident 10°, 30°, and 90° relative to broadside
receive bandwidth	12 kHz
I/Q sampling rate	40 kHz
algorithm parameters	50-sample block length (2 ms), 5-block averaging time constant (10 ms)

In these tests, SIR(in) was varied for particular combinations of RF frequency, jamming direction, and adaptive algorithm. The bit error rate (BER) was recorded as a function of SIR(in), and the values of SIR(in) at which the BER rose above an acceptable level noted. It was observed that as SIR(in) was decreased from 0 dB down to -40 dB, the BER first decreased (as a result of the expected greater effectiveness of the adaptive algorithm against stronger jamming signals) then reached a minimum, after which it began to increase (as a result of the limited processing gain due to differential frequency-response effects). A bit error rate of 10^{-2} is considered to be the maximum rate for most low-overhead error-correction techniques to be effective. This was taken to be the maximum acceptable BER for these tests. From plots of BER vs. SIR(in), the minimum and maximum values of SIR(in) between which the BER was less than 10^{-2} were recorded.

Each combination of RF frequency and jamming-signal direction corresponded to a

specific difference between antennas, in the relative phase of the desired and jamming signals (see Table 5.3). The minimum and maximum values for which the BER was below threshold is plotted as a function of the relative phase difference for both the PRI and EV algorithms, in Figure 5.12. (The smaller relative phase differences (those corresponding to a 10° jamming direction) did not permit a BER below 10^{-2}, and so could not be included in this figure.)

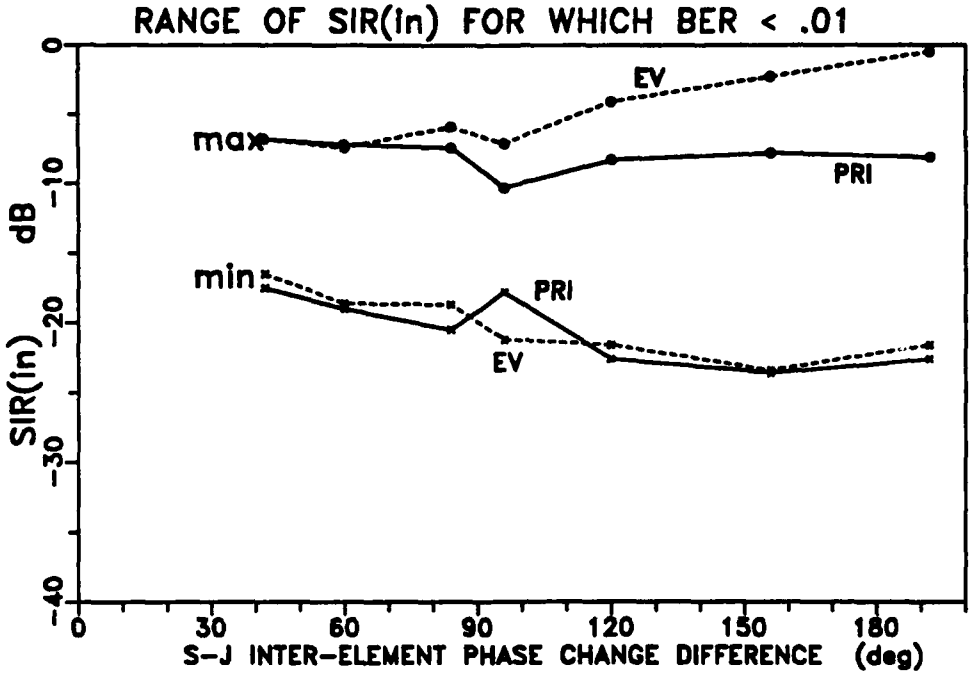

Figure 5.12 Range of SIR(in) for which BER < 10^{-2}, as a function of the difference between antennas in the relative phase of the wanted and jamming signals, for the PRI and EV algorithms operating against noise jamming.

In Figure 5.12, it can be seen that the effective operating range of the PRI algorithm implemented on the present hardware does not vary greatly over the range of differences in relative phase plotted, except for a slight widening at the larger relative phase differences corresponding to a slight drop in the minimum SIR(in) from approximately -19 to -24 dB. The maximum SIR(in) for successful operation remains constant at approximately -9 dB. From the power-inversion properties of the PRI algorithm, this corresponds to SIR(out) of +9 dB, which is consistent with a BER of 10^{-2} for FSK signals.

The operating range of the EV algorithm, on the other hand, is observed to increase significantly as the difference in relative phase is increased. This is due not only to a slight decrease in the minimum acceptable SIR(in) similar to that experienced by the PRI algorithm, but also a substantial increase in the maximum SIR(in) from -9 dB to nearly 0 dB. This increase is consistent with the greater ability of the EV algorithm to separate signals which are close in power, provided that their input-signal vectors are more orthogonal than parallel.

In practice, there will be times when the interfering signals lie outside the range for acceptable operation, as experienced by the present system. The limited operating range experienced, especially for the PRI algorithm but also the EV algorithm, points out the need for other algorithms which exploit known features of the communications signals, thereby permitting effective operation at nearly-equal jamming and wanted-signal powers, under all conditions. Improvements in the channel differential frequency-response matching are also required, along with greater digital precision (an increase from 12-bit to 16-bit D/A conversion), as this will permit effective operation against much stronger jamming signals (i.e., low SIR(in)).

5.3 TESTS WITH OVER-THE-AIR SIGNALS

Laboratory tests permitted a detailed evaluation of performance, since the input-signal levels could be easily controlled, both in amplitude and in (simulated) arrival direction. Over-the-air tests do not permit such easy assessment. Over-the-air incoming signals are subject to multipath effects, with the result that the apparent directions and amplitudes depend on the local conditions as well as the original signal directions and so may differ between antenna elements and change with the RF frequency used. Despite the difficulties of performance assessment, it is important to perform over-the-air tests to demonstrate the functioning of the system with real-world signals and to ensure that real-world operations do not introduce any adverse influences on performance beyond those observed in the lab.

Over-the-air tests of the adaptive antenna system operating with the PRI and EV algorithms were performed using the FSK communications signal and noise-jamming signal of Section 5.2.3. The experimental arrangement was similar to that of Figure 5.5, with the RF signal distribution system replaced by transmitting and receiving antennas located on the roof of the laboratory.

The rooftop antenna arrangement is shown in Figure 5.13. The receiving antennas consisted of four Harris 3013/VRC vertical whip antennas, 2.5 m in height, mounted on an aluminum ground plane in a square array, 2 m on a side. This geometry was similar to the simulated array of the in-lab tests. Two receive antennas were selected at a time, for operations. The aluminum ground plane was raised approximately 1 m above the roof, close to the level of the masonry railing along the edge of the roof. Transmitting antennas (also Harris 3013/VRC vertical whips), placed approximately 10 m away at a similar height, were used for the communications and jamming signals. A rooftop penthouse located nearby provided an obvious source of multipath propagation for both communications and jamming signals. Other obvious local features contributing to multipath included the railing, a 2-m-high chain-link fence behind one of the transmitting antennas, and an external metal stairway to the penthouse roof. The transmitters and receiving system were situated in a basement laboratory of the three-story building. Matched-length cables approximately 100 m long were installed between the rooftop and laboratory, to pass the transmitted signals to their antennas, and bring signals from the receive antennas to the receivers.

For the tests reported here, receiving antennas A and B were used. The input signal levels seen by the adaptive-antenna processing system were measured at the processor output by

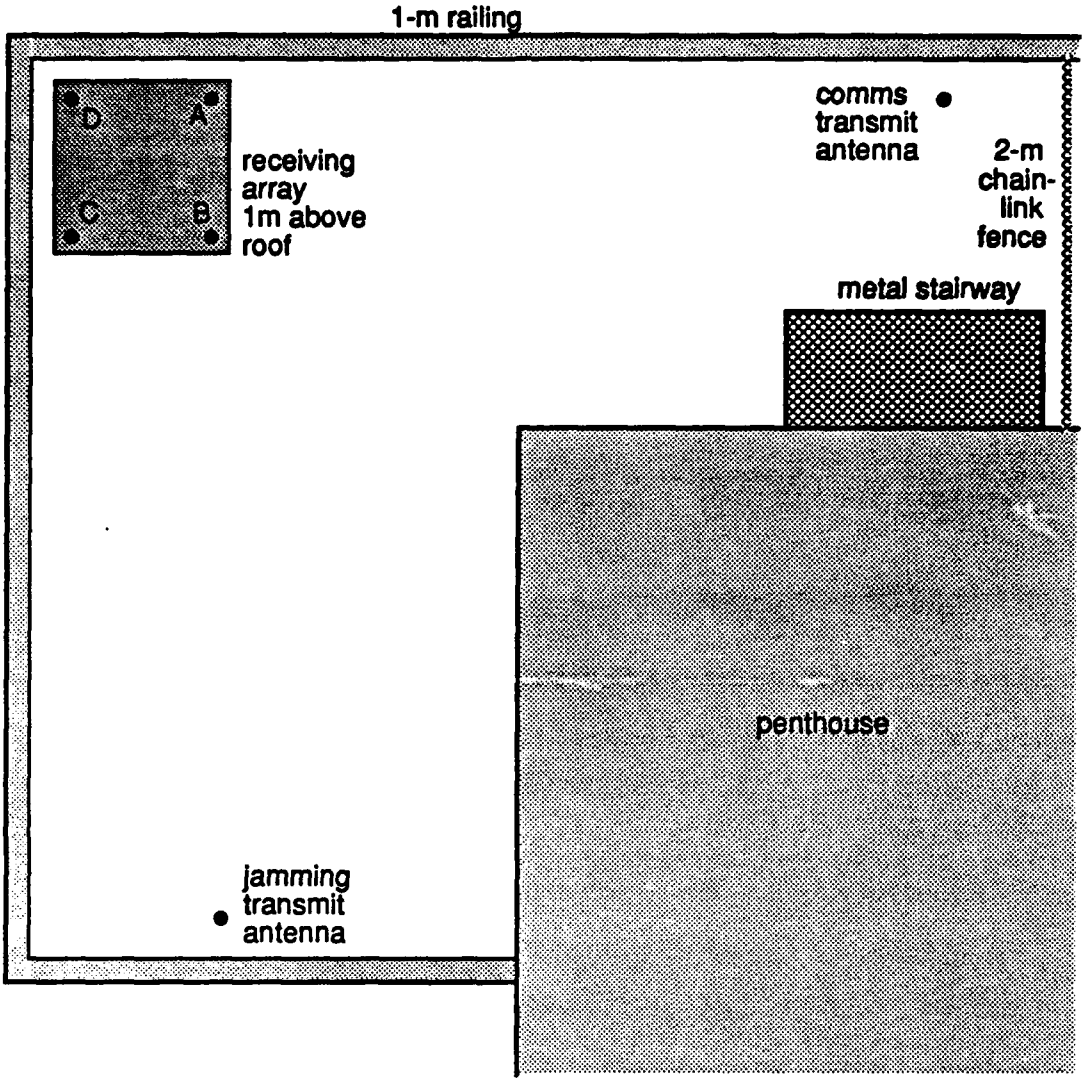

Figure 5.13 Rooftop antenna arrangement for over-the-air tests.

running the array with fixed weights, selected to pass a particular input antenna's signals to the output without change (antenna A, fixed weights (1, 0); antenna B, fixed weights (0,1)). The operating frequencies had to be changed slightly from the in-lab tests, to channels which were not already occupied (35, 49.5, and 77.5 MHz).

The signals used were similar to those described in Table 5.4, Section 5.2.3 for the in-lab tests. A 2.4-kb/s FSK data signal was employed as the communications, and bandwidth-limited white noise as the jamming. The transmitted signal levels were adjusted so that the receive signal levels were similar to those experienced in the in-lab tests. The communications and jamming signal levels were initially set to similar levels, and the communications level was adjusted downwards so as to cover an input signal-to-jamming ratio SIR(in) from 0 to -40 dB. The bit error rate (BER) was recorded as a function of SIR(in) for the three transmitted frequencies.

Figure 5.14 shows the resultant BER achieved as a function of SIR(in) from antenna B, for the PRI and EV algorithms. Also shown on this figure is a dotted line representing the maximum BER (10^{-2}) permitted for acceptable communications. The general behaviour revealed by these plots can be described as follows: As SIR(in) was reduced below 0 dB, SIR(out) became high enough to permit the bit-error-rate analyzer to synchronize to the transmitted data and a bit error rate to be recorded. When SIR(in) was reduced further, the BER dropped into the range of acceptable communications (< 10^{-2}). (As seen in this figure, it did not decrease to zero, due to an occasional data conversion problem in the output D/A portion of the processing system, which set a lower limit to the achievable BER near 0.4 x 10^{-2}. A correctly functioning operational system

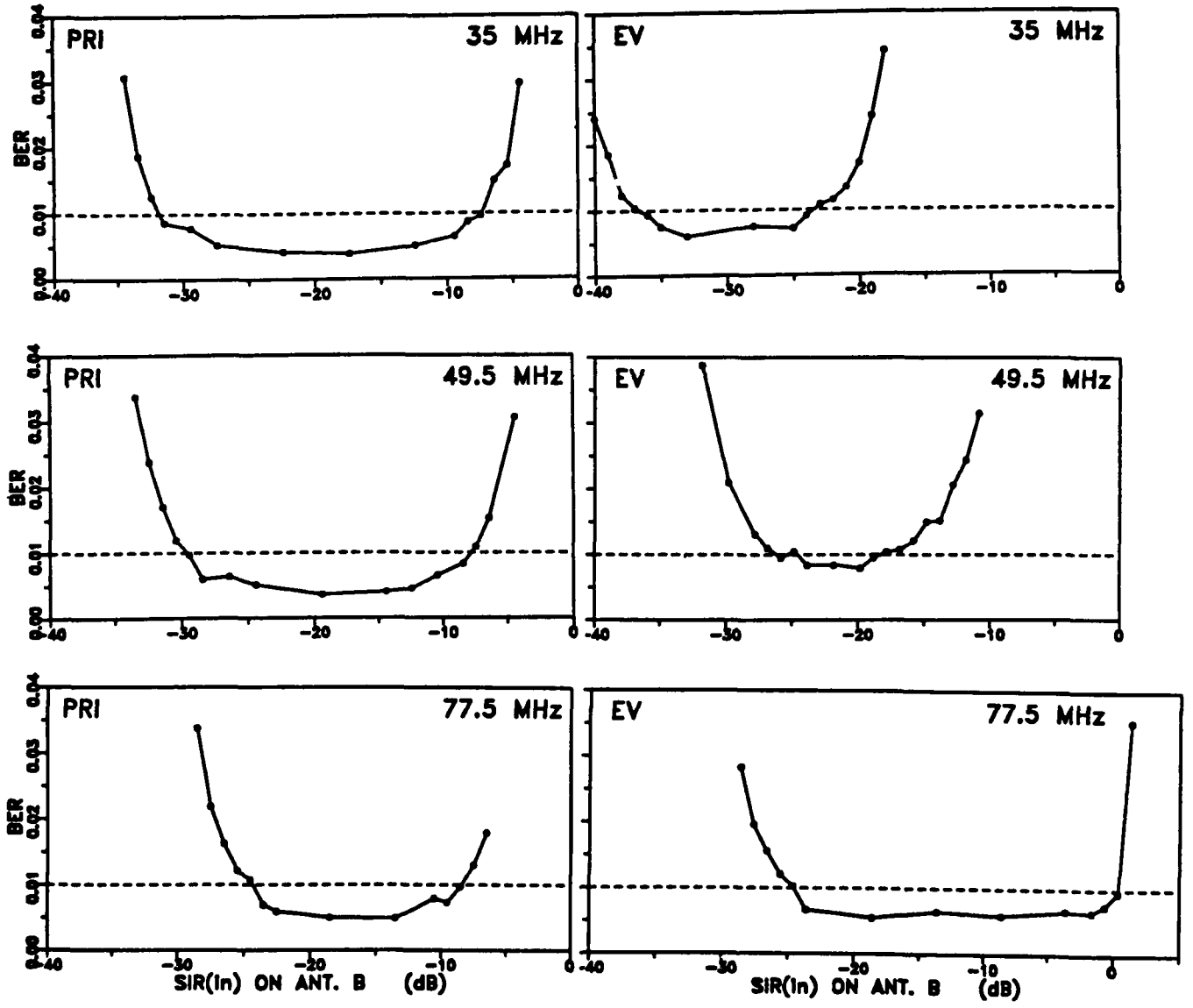

Figure 5.14 BER as a function of the SIR(in) observed at antenna B, for the over-the-air tests of the adaptive antenna system operating with the PRI and EV algorithms, at RF frequencies of 35, 49.5, and 77.5 MHz.

will not have this problem.) With further reductions in SIR(in), the BER eventually began to increase, and passed above the maximum permitted for acceptable communications.

It was observed in these tests, that the input signal-to-jamming ratio SIR(in) differed significantly between the two antennas. At 35 MHz, a large difference was seen between antenna A and B in this ratio (-13.2 dB). A slightly smaller difference (-10.9dB) was seen at 49.5 MHz, and a much smaller (reversed) difference (+2.4 dB) was seen at 77.5 MHz. These changes are consistent with antenna B shielding antenna A from the jamming signal (See Figure 5.13), particularly at the lower frequencies, and the shielding being mitigated by multipath propagation which was most felt at the highest frequency.

In the in-lab tests it was seen that the PRI algorithm performance was approximately the power inversion expected from theory, when SIR(in) was between 0 and -15 dB. From theory, the PRI algorithm inverts the relative input power levels seen at the antenna to which the variable weight is applied (antenna B in this case). From Figure 5.14, the point at which communications first becomes acceptable, as SIR(in) is reduced, is the same (measured on antenna B) for all three frequencies with the PRI algorithm, near -8 dB. This agrees with theory, since an inverted output power ratio SIR(out) near +8 dB, is consistent with an instantaneous BER of 10^{-2} for FSK signals.

The actual values of SIR(out) for which the BER dropped below 10^{-2}, for the PRI algorithm, were found to be 10 and 11 dB for RF frequencies 49.5 and 77.5 MHz respectively. These greater-than-expected values for SIR(out) at the threshold BER may be due to the fact that the weights and thus the instantaneous values of SIR(out) were fluctuating in response to statistically-varying signals while the BER recordings were made. Any significant fluctuations toward smaller values of SIR(out) would be expected to greatly increase the instantaneous BER, while same-size fluctuations towards larger values of SIR(out) would decrease BER only slightly. Thus the mean SIR(out) corresponding to a mean BER of 10^{-2} is expected to be somewhat higher than the corresponding instantaneous value. The measured values are thus consistent with the measured BER, and slightly higher than the values expected from power inversion.

The fact that the PRI performance is related to the input-signal ratio at a particular antenna may be exploited. By switching antennas in response to changing conditions, so that the variable weight is always applied to the antenna with the lowest input ratio SIR(in), the operating range of the PRI algorithm may be extended, particularly in cases where one antenna may be shielding the other, or multipath propagation is present.

The range of values of SIR(in) over which the PRI algorithm was observed to permit acceptable communications is seen in Figure 5.14 to differ somewhat from the two lower RF frequencies to the higher frequency. The minimum SIR(in) (as measured on antenna B) increases from roughly -30 dB at 35 and 49.5 MHz, to -25 dB at 77.5 MHz. A minimum SIR(in) of -30 dB corresponds to a maximum processing gain near 38 dB, while a minimum SIR(in) of -25 dB corresponds to a maximum processing gain near 33 dB. The maximum processing gain expected on the assumption of identical antennas, was seen in Section 5.1 to be 35 dB, as set by the differential frequency response of the channels. Considering the different responses of the actual antennas to the communications and jamming signals, and their variation with frequency, the 38 and 33-dB maximum gains inferred appear reasonable.

The EV algorithm performance is less predictable. It can be seen from Figure 5.14 that the range of values of SIR(in) (as measured on antenna B), for which acceptable communications was achieved, depends greatly on frequency. Unlike PRI, SIR(out) for the EV algorithm cannot be expected to be solely dependent on SIR(in) seen at a single antenna. Instead it depends in a more complex way on the relative amplitudes of the signals as seen at both antennas, and their phases. The range of SIR(in) for acceptable communications with the EV algorithm was observed in these tests to be considerably less, at the two lower frequencies, than that achieved with the PRI algorithm. This is somewhat disappointing, given the better performance expected for the EV algorithm from theory [2]. The unexpectedly smaller operating range occurs at the two frequencies (35 and 49.5 MHz) where the input signal ratio SIR(in) differed significantly between antennas, a condition which was not considered in the theory. At the remaining frequency (77.5 MHz), the operating range with EV is much better than with PRI.

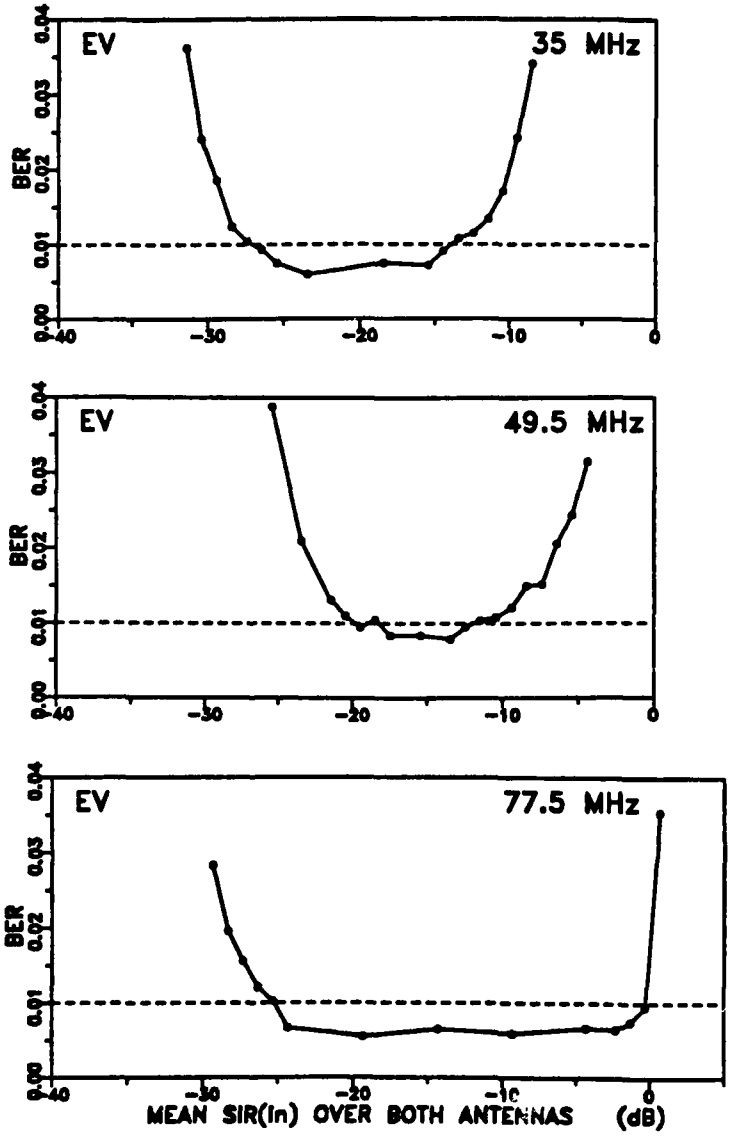

Figure 5.15 BER as a function of SIR(in) based on the mean input powers over the two antennas, for the EV algorithm, at RF frequencies of 35, 49.5 and 77.5 MHz.

A better approach to displaying the BER achieved with the EV algorithm may be as a function of SIR(in) taken from the mean signal powers over both antennas. This is implemented in Figure 5.15.

In this figure, as SIR(in) is reduced, the point at which communications first becomes acceptable is seen to depend on the RF frequency: -13 dB at 35 MHz, -11 dB at 49.5 MHz, and -1 dB at 77.5 MHz.

The communications transmitting antenna was broadside to receiving pair (A and B in Figure 5.13), and the jamming transmitting antenna was 90° off. Under these conditions, if multipath propagation is neglected, the input vectors for the communications and jamming signals are expected to be nearly orthogonal at 77.5 MHz RF, provided both antennas experience near-similar SIR(in) which is the case at this frequency. For the EV algorithm operating under these conditions, the maximum SIR(in) for acceptable communications is expected to approach 0 dB. As a result of this upwards extension of allowed SIR(in), the operating range for the EV algorithm was noted to exceed that of the PRI algorithm at 77.5 MHz RF, even in the difficult multipath situation tested. (As previously indicated, this did not occur at the 35 and 49.5 MHz RF operating frequencies.)

In summary, the over-the-air tests reveal some unexpected performance effects which can arise in a real situation. The EV algorithm performed worse at the two lower frequencies than the PRI algorithm despite its predictably better performance at the highest frequency. This is surprising, given the better performance predicted by the theory and simulations for similar antennas. The antennas did not fit the theoretical criterion at the lower frequencies, as they experienced significantly different input ratios SIR(in), due mainly to the shielding of one antenna by the other in some directions. The EV algorithm, more than the PRI algorithm, appears susceptible to performance deterioration in such a situation. The reason for this remains to be determined.

The PRI algorithm performed predictably, with its output ratio SIR(out) close to the predicted power inversion of the signals seen by the antenna to which the variable weight was applied, provided the gain required fell below the limit set by the differential frequency response of the input channels. In situations such as that tested, where the antennas can experience significantly different SIR(in), the operating range of the PRI algorithm could be extended by switching antennas so that the variable weight is always applied to the antenna with the lowest SIR(in).

6.0 CONCLUSIONS AND RECOMMENDATIONS

The present work provided an investigation of the implementation issues for a VHF adaptive-antenna system as well as the potential performance of a particular class of adaptive-antenna algorithms. This was achieved through the development of a VHF adaptive-antenna test bed, including a programmable adaptive antenna processing system. A programmable implementation is recommended, in view of the potential need to incorporate a number of adaptive algorithms for receiving different types of signals or meeting different threats, and to permit future modification.

As was demonstrated by the test-bed system, the implemented technology is easily capable of providing the required programmability and processing speeds to handle VHF signal bandwidths, and computation-intensive adaptive algorithms, for a two-antenna system. Technology advances in the four years since the technology was selected have been significant, so that a four-antenna VHF implementation should not pose any problem, should this be considered desirable.

Several weaknesses were found in the system as implemented.

The main limit to the performance of the adaptive antenna system was in the differential frequency response of the receivers set by the final-stage filtering which limited the bandwidth of the signals which could be received. Despite the fact that the present system used precision filters for this purpose, this effect limited the null depths achievable by the system against jamming or interference, which occupied the full receive bandwidth, to -35 dB. This problem can be reduced substantially in future systems by digitizing the signal at IF and performing the downconversion to baseband and final-stage filtering digitally, thus eliminating any mismatches in the final filters.

Another limit to performance for an adaptive antenna system is the receiver phase noise, which also impacts on the null depth achievable, when the input receivers are kept phase coherent through the use of a common frequency standard (as was done in the present system). In the present system, which used Watkins-Johnson WJ-8628A-1 receivers selected for their low phase noise, the null depth achievable was limited to -48 dB by this effect. This limitation can be eliminated by using common local oscillator signals for all receivers, so that the phase noise remains coherent between receivers and can thus be cancelled, along with the stronger interfering signals.

A third limit to performance in any digital system is the quantization noise introduced by the A/D conversion of the signals. For the present system, 12-bit A/D converters were used, which limited the null depth to at least -65 dB, assuming that there was no offset error in the conversion process. With assumed offset errors as large as two bits, the null depthwould be limited to -47 dB. The quantization noise will be reduced, if finer quantization is used. 16-bit A/D converters having the required sampling rates are now readily available and should be used.

A related concern is the need for a common AGC for the input receivers. This was not implemented in the present test bed, but is a concern in practice where the range of received signals could exceed the fixed-gain dynamic range of the receivers and A/D converters. The AGC

switching process is made easier if more bits are available, so that the signal need not occupy all the available bits of the A/D converter and still be adequately represented. For this reason also, 16-bits-or-higher A/D conversion is recommended in future VHF systems.

The adaptive-antenna algorithms tested in the present work were restricted to those not requiring a priori information about the signals being received, and to two-element arrays. (Adaptive-antenna land-mobile implementations are expected to be restricted mainly to two antennas, owing to limited space and portability requirements.) The tested algorithms had the effect of separating the incoming signals on the array into different output channels.

The first algorithm implemented was the PRI algorithm, whose theoretical performance was that of power inversion. The relative strength of the interfering and wanted signal seen at the input was expected to be inverted in one output channel, and maintained as seen at the input, in the other output channel. Most communications signals require a signal-to-interference ratio of the order of 8 dB or so for adequate performance. The PRI algorithm will not cancel interference adequately in these cases, when the interference is within 8 dB of the communications. Such situations are quite likely in practice, owing to the fading nature of mobile communications, and the wide range of signal levels anticipated, owing to the strong dependence of signal strength upon distance and local terrain. When the interference is increased more than 8 dB above the communications, the power inversion permits adequate communications. However, as observed in the implementation, the null depth limits set by the various effects mentioned above, particularly the differential frequency response of the receivers, sets an upper limit to how much stronger the interference can be than the communications and still be adequately cancelled. In the present system, this limit was observed to be of the order of 20 to 25 dB, which is less than the range of signal strengths that could be expected in practice.

Eigenvector weighting was implemented in the EV algorithm. The theoretical performance for this technique has been shown to be everywhere better than that of power ratio inversion under the assumption of identical array element patterns, approaching that of PRI for close jamming and wanted-signal directions, and being substantially better than PRI when the directions are well-separated [2]. The two-element EV implementation tested in the present work showed these properties. It permitted a greater successful operating range (in terms of input signal-to-interference ratio SIR(in)) with FSK signals, when the relative phase change difference between antennas for the jamming and communications signals lay between 90 and 180°. This corresponds to more than half the possible direction combinations, for an element spacing of one-half wavelength. (The theory indicates that the range of directions showing a performance substantially better than PRI increases with the number of antennas used [2]. Thus EV performance will improve if more antennas can be used.) Nonetheless, there was a substantial range of directions and jamming levels close to that of the communications signal, where the EV algorithm would not adequately cancel the jamming. Like the PRI algorithm, the null depth limits of the equipment placed an upper limit on the strength of the jamming that could be adequately cancelled by the EV algorithm, to 20 to 25 dB above the communications.

The signal separation techniques implemented here in two-element form were found to be limited, both theoretically and practically, in the range of operating conditions over which they could cancel interference adequately. In order to remedy this situation, it is necessary to invoke

adaptive algorithms that exploit predetermined properties of the signals being received. The newer signal structures being implemented for data communications can be readily handled by such techniques, since they contain predetermined embedded code (intended for synchronization, identification, and the like), which can be exploited to obtain a 'reference' signal to match the adapted output to. Unlike signal separation techniques, reference-based adaptive algorithms do not have a lower limit on the strength of the jamming signal that can be adequately cancelled.

Future work in VHF adaptive antenna development will be carried out under an existing technology base program. This work will concentrate on correcting identified deficiencies, and on extending the range of algorithms and applications considered.

Immediate plans for the next year include a replacement of the programmable processing system with a low-cost system based on technology which has only recently become available. The new system will use a PC computer as host, and a single-board TMS320C40-based two-channel signal processing system, to implement two-element adaptive-antenna algorithms. In addition to performing the adaptive-antenna algorithms, this board will perform the final-stage frequency downconversion and filtering in digital form, thereby reducing differential-frequency-response null-depth limiting substantially. It also incorporates 16-bit A/D conversion, which should provide a greater operating range and reduce quantization noise. Its compactness makes it a candidate for operational implementation, as well. The present VHF receivers will be used, but will be run from common local oscillators rather than a frequency standard, in order to remove phase-noise effects.

Reference-based algorithms have been developed for HF applications under a separate task. These algorithms take advantage of time-division-multiplexed code embedded in the phase-shift-keyed communications signals. It is planned to adapt these algorithms to VHF communications signals of similar structure, and implement them in two-element form on the new adaptive-antenna processing system. Such signals are appropriate for integrated voice/data communications and packet switching, and can be implemented in fixed-frequency or frequency-hopping versions. These cases will be considered as requirements and resources permit.

REFERENCES

[1] Horowitz, L., Blatt, H., Brodsky, W., and Senne, K. (1979)
Controlling Antenna Arrays with the Sample Matrix Inversion Algorithm.
IEEE Transactions on Aerospace and Electronic Systems, **AES-15**, 6 (1979), 840-847.

[2] Jenkins, R.W., and Moreland, K.W. (1993)
A Comparison of the Eigenvector Weighting and Gram-Schmidt Adaptive Antenna Techniques.
IEEE Transactions on Aerospace and Electronic Systems, **AES-28**, 2 (1993), 568-575.

[3] Summers, A. (1986)
Performance Specification for PV 2413A Universal Interference Cancelling Equipment.
unpublished report 630/SM/29849, Plessey PLC., 1986.

[4] Hackett, C.M., Jr., (1981)
Adaptive Arrays Can be Used to Separate Communication Signals.
IEEE Transactions on Aerospace and Electronic Systems, **AES-17**, 2 (1981), 234-247.

[5] Rohde, U.L. (1983)
Digital PLL Frequency Synthesizers.
Englewood Cliffs NJ: Prentice-Hall, 1983, pp. 69-72.

DOCUMENT CONTROL DATA

(Security classification of title, body of abstract and indexing annotation must be entered when the overall document is classified)

1. ORIGINATOR (the name and address of the organization preparing the document. Organizations for whom the document was prepared, e.g. Establishment sponsoring a contractor's report, or tasking agency, are entered in section 8.)

COMMUNICATIONS RESEARCH CENTRE
P.O. BOX 11490, STATION H
OTTAWA, ONTARIO K2H 8S2

2. SECURITY CLASSIFICATION (overall security classification of the document. including special warning terms if applicable)

UNCLASSIFIED

3. TITLE (the complete document title as indicated on the title page. Its classification should be indicated by the appropriate abbreviation (S,C or U) in parentheses after the title.)

VHF ADAPTIVE ANTENNA DEVELOPMENT TASK: FINAL REPORT (U)

4. AUTHORS (Last name, first name, middle initial)

JENKINS, ROBERT W., TENNE-SENS, U. ANDREJ, LISSON, BRIAN

5. DATE OF PUBLICATION (month and year of publication of document)

JUNE, 1993

6a. NO. OF PAGES (total containing information. Include Annexes, Appendices, etc.)

65

6b. NO. OF REFS (total cited in document)

4

7. DESCRIPTIVE NOTES (the category of the document, e.g. technical report, technical note or memorandum. If appropriate, enter the type of report, e.g. interim, progress, summary, annual or final. Give the inclusive dates when a specific reporting period is covered.)

Final Report

8. SPONSORING ACTIVITY (the name of the department project office or laboratory sponsoring the research and development. Include the address.)

DEFENCE RESEARCH ESTABLISHMENT OTTAWA
3701 CARLING AVENUE
OTTAWA, ONTARIO

9a. PROJECT OR GRANT NO. (if appropriate, the applicable research and development project or grant number under which the document was written. Please specify whether project or grant)

1410-0417W

9b. CONTRACT NO. (if appropriate, the applicable number under which the document was written)

10a. ORIGINATOR'S DOCUMENT NUMBER (the official document number by which the document is identified by the originating activity. This number must be unique to this document.)

CRC REPORT # 93-003

10b. OTHER DOCUMENT NOS. (Any other numbers which may be assigned this document either by the originator or by the sponsor)

11. DOCUMENT AVAILABILITY (any limitations on further dissemination of the document, other than those imposed by security classification)

(X) Unlimited distribution
( ) Distribution limited to defence departments and defence contractors; further distribution only as approved
( ) Distribution limited to defence departments and Canadian defence contractors; further distribution only as approved
( ) Distribution limited to government departments and agencies; further distribution only as approved
( ) Distribution limited to defence departments; further distribution only as approved
( ) Other (please specify):

12. DOCUMENT ANNOUNCEMENT (any limitation to the bibliographic announcement of this document. This will normally correspond to the Document Availability (11). However, where further distribution (beyond the audience specified in 11) is possible, a wider announcement audience may be selected.)

UNCLASSIFIED

SECURITY CLASSIFICATION OF FORM

13. ABSTRACT (a brief and factual summary of the document. It may also appear elsewhere in the body of the document itself. It is highly desirable that the abstract of classified documents be unclassified. Each paragraph of the abstract shall begin with an indication of the security classification of the information in the paragraph (unless the document itself is unclassified) represented as (S), (C), or (U). It is not necessary to include here abstracts in both offical languages unless the text is bilingual).

The work of the VHF adaptive antenna development task is reported. An adaptive-antenna test bed was assembled, including a programmable real-time signal processing system. Power-ratio inversion (PRI) and eigenvector-weighting (EV) adaptive algorithms were investigated analytically and by means of simulation, and implemented in two-element form on the real-time processor. These algorithms tend to separate incoming signals into different output channels according to their relative strengths, and do not require a priori information on the communications being received.

The PRI algorithm was expected to invert the relative input powers of the jamming and communications signal, in the output signal. Analyses indicated that the EV algorithm should perform better than the PRI algorithm, especailly when the incoming jamming and communications signal are well-separated in direction. Tests with real-world signals revealed deficiencies in the hardware implementation, as well as limitations in the algorithms themselves. Means of correcting the deficiencies are identified, and proposed for a new real-time signal processor to be implemented as part of a continuing technology-base activity. More effective algorithms which make use of a priori information on the communications signal to obtain a reference signal are recommended for implementation in the continuing work, the goal of which is to produce a demonstrable effective VHF adaptive antenna system for land tactical communications.

14. KEYWORDS, DESCRIPTORS or IDENTIFIERS (technically meaningful terms or short phrases that characterize a document and could be helpful in cataloguing the document. They should be selected so that no security classification is required. Identifiers, such as equipment model designation, trade name, military project code name, geographic location may also be included. If possible keywords should be selected from a published thesaurus. e.g. Thesaurus of Engineering and Scientific Terms (TEST) and that thesaurus-identified. If it is not possible to select indexing terms which are Unclassified, the classification of each should be indicated as with the title.)

adaptive antennas,
VHF Communications

UNCLASSIFIED

SECURITY CLASSIFICATION OF FORM